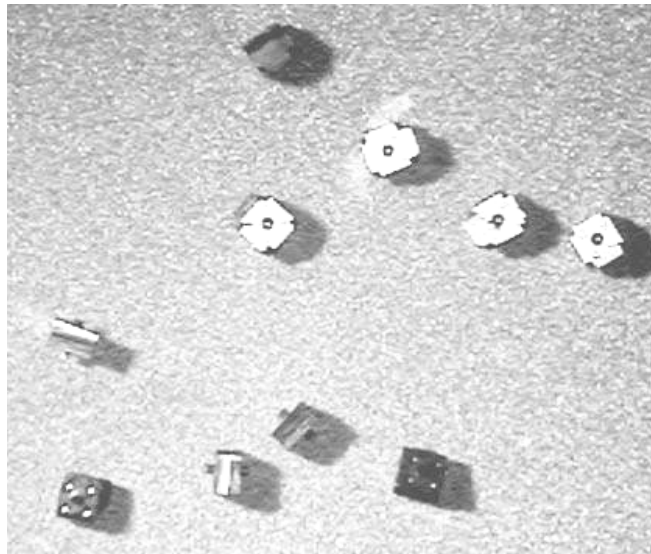


Diploma Thesis, Micro Engineering
Winter 2005/2006

EXPERIMENTAL SETUP FOR SELF-ASSEMBLY ANALYSIS AND MODELING



Student:	Professors:	Coaching and Supervision:
Madeleine Kaegi madeleine.kaegi@epfl.ch Tel. +41 764287201	Hannes Bleuler, EPFL Hannes.bleuler@epfl.ch Karl F. Böhringer, University of Washington karl@ee.washington.edu	Jean-Marc Breguet, EPFL Jean-marc.breguet@epfl.ch Sangjun Park, University of Washington park@ee.washington.edu

▪ ACKNOWLEDEGMENT

I am grateful to professor Böhringer for giving me this wonderful opportunity to do my diploma thesis as a member of the MEMS group at the University of Washington in Seattle. Thanks for supporting me and to motivate me especially during the end phase of the work. A special thank to Dr. Breguet at EPFL for coordinating this project and for his encouragement.

I also want to acknowledge all the members of the MEMS group, especially Neil, for the introduction to the lab equipment and the inspiring discussions and Sangjun, for doing the production of the cubes. I thank professor Klavins, Crystal and Nils for the discussions and their suggestions during the Self-Assembly group meetings.

Seattle, February 23rd 2006

Madeleine Kägi



Adresse postale : **EPFL LSRO**
Station 9
CH 1015 Lausanne

MASTER PROJECT WINTER 2005-2006

Title: Experimental Setup for Self-assembly Analysis and Modeling
Candidate: Madeleine KAEGI **Section:** Micro Engineering
Professors: Hannes Bleuler (EPFL), Karl F Böhringer (UW)
Assistants: Jean-Marc Breguet (EPFL), Sangjun Park (UW)

Context:

The University of Washington is investigating the fundamental principles of self-assembly processes for the massively parallel manufacture of engineered systems at the micro to nano scale in the frame of an NSF project.

In her Master project, the candidate will have to develop a second generation experimental setup. It consists essentially of a “shaker” capable of simulating “Brownian movements” of the micro-parts, typically $200\mu\text{m}$ to $500\mu\text{m}$ Si cubes, to be self-assembled. The setup must contain the essential features for this study, while being general enough to be applicable to a wide range of self-assembly scenarios and simple enough to allow experiments with fast turn-around.

Objectives:

- design and build a new experimental setup based on the expertise gained with the first prototype;
- run a sequence of experiments with micro-scale self-assembling parts (typically $200\mu\text{m}$ to $500\mu\text{m}$ Si cubes);
- observe assembly performance as a function of various system parameters;
- continue to develop a model that relates system parameters to performance parameters.

Deliverables:

- prototype of the “shaker” with its controller and user interface allowing easy operation;
- characterization of the prototype (obtained movements for various excitations frequencies, input signals, ...);
- analysis of self-assembly process for various systems parameters. A first tentative model will be proposed if time allows.

Notes

- Detailed specifications for the “shaker” will be given by UW to the candidate at least two weeks before the project begins. The candidate and her assistant at EPFL will make a first evaluation of the most appropriate technology, before leaving for the USA.
- Five copies of the report have to be submitted not later than February 24th at noon. The reports include a one page summary. The candidate will present her work at EPFL (25 minutes of presentation and 20 minutes of discussion) during the week 11.

The Professors:

The assistants:

Hannes Bleuler, Karl Böhringer

Jean-Marc Breguet, Sangjun Park

Experimental Setup for Self-Assembly

Experimental Setup for Self-Assembly Analysis and Modeling
Madeleine Kägi, Microtechnique

Professor : Hannes Bleuler, Karl Böhringer
Assistants : Jean-Marc Breguet, Sangjun Park

Self-Assembly is a stochastic process, in which basic units form a structure using interaction between each other.

This thesis consists of designing the experimental setup for Self-Assembly experiments and modeling the Self-Assembly process.

In the experiments, two different types of silicon cubes are agitated in a confined space. The dimension length of a cube is 635 μm.

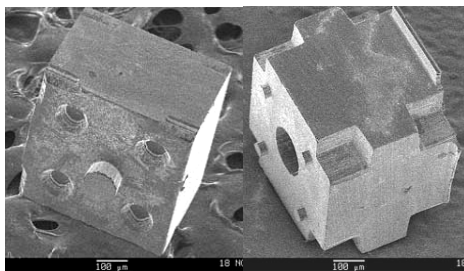


Fig 1: Type_1 and Type_2 cubes

Cubes bind to each other when two adjacent surfaces come close to each other and their binding forces dominate the agitation forces.

A voice coil speaker provides the energy for the Self-Assembly process. On the speaker, an aluminum platform is mounted rigidly. The platform supports a silicon stage with a glass tube and an accelerometer.

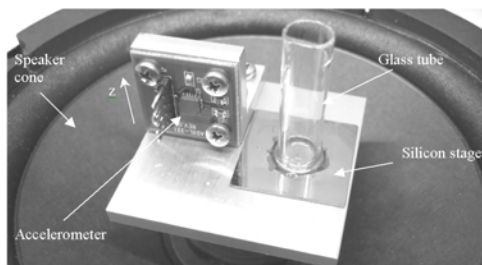


Fig 2: setup

The accelerometer provides the data to establish the characteristics of the setup.

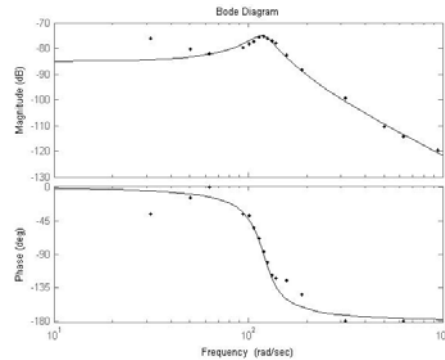


Fig 3: gain and phase versus frequency

$$H(s) = \frac{z(s)}{U(s)} = \frac{4.47 \cdot 10^{-4}}{7.82 \cdot 10^{-5} s^2 + 5.31 \cdot 10^{-3} s + 1}$$

The *cutoff frequency* of the system is at 19 Hz (=119 rad/s)

The *model of the Self-Assembly process* is assumed to be analog to the *thermodynamics* of chemical reactions.

The *state of the system* consists of a vector u :

$$\vec{u} = \begin{pmatrix} u_1 \\ u_2 \\ \vdots \\ u_k \end{pmatrix}$$

- u_i : number of assemblies of type i
- G_u : free energy assigned to the state u
- G_v : free energy assigned to the state v
- $k_{u,v}$: rate at which the state u transforms to v
- $k_{v,u}$: rate at which the state v transforms to u

The thermodynamic equation establishes the dependency of the energies of the states and the assembly rates:

$$\frac{k_{v,u}}{k_{u,v}} = \exp\left(\frac{-(G_u - G_v)}{E_T}\right)$$

The theoretical model has not been verified, since the assembly experiments are not successful so far; no cubes assembled. This demonstrates that the *difference of the free energies* from u to v is not high enough.

▪ TABLE OF CONTENTS

1. INTRODUCTION	6
1.1 Definition of Self-Assembly	6
1.2 Aim of the NSF 3D Self-Assembly project	7
2. APPROACH TO THE SELF-ASSEMBLY EXPERIMENTS	8
2.1 Design of the assembling components	8
2.2 Design of the stage	10
2.3 Model of the Self-Assembly process	11
3. DESIGN OF THE EXPERIMENTAL SETUP	12
3.1 Solution catalog and choice	12
3.2 Speaker	14
3.3 Sensor research	17
3.4 Mechanical parts	19
3.5 Setup Assembly	20
4. SETUP CHARACTERIZATION	21
4.1 Measuring arrangement	21
4.2 Results	26
4.3 Energy model	31
5. RESULTS OF THE EXPERIMENTS	35
5.1 Observations	35
5.2 Identification of the model parameters	37
5.3 Part density	39
6. CONCLUSION	40
7. REFERENCES	41
8. APPENDIX	42

1. INTRODUCTION

This diploma thesis is part of the NSF¹ 3D Self-Assembly project at the University of Washington in Seattle. The MEMS² research group at the University of Washington has worked on a number of Self-Assembly projects so far³.

This NSF 3D Self-Assembly project aims to assemble three-dimensional silicon cubes in a dry environment.

The main part of the thesis consists of designing the experimental setup and of elaborating its characteristics. The Self-Assembly process will be analyzed and a model will be established to predict the Self-Assembly performance.

1.1 Definition of Self-Assembly

Self-Assembly is a phenomenon in which basic units form a structure using interaction between each other. Various driving forces have been employed for Self-Assembly, especially Van der Waal forces, liquid surface tension, electrostatic and magnetic forces.

By definition Self-Assembly is a spontaneous process that occurs in a *statistical*, non-guided fashion. It is observed in nature on a small scale: crystal growth, biological membrane and micelle formation and DNA replication. Self-Assembly is quite common in the biological world: three-dimensional complex structures are often formed using *interfacial interaction* and *shape selective recognition*.

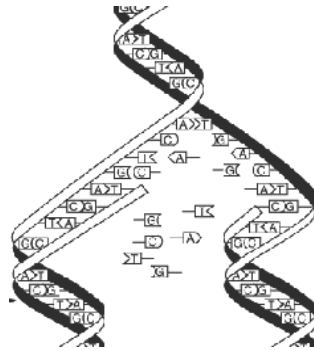


Figure 1: [9] Self-Assembly in nature: DNA replication

Self-Assembly techniques enable mass packaging at practical time frames. Current Self-Assembly techniques for meso scale (roughly, 100's of nm to 100's of μm) flat parts are based on two major mechanisms: capillary-driven Self-Assembly and shape-directed Self-Assembly.

Several research groups have developed *capillary-driven* Self-Assembly processes in water environments, where liquid droplets on receptor sites attract and align parts by minimizing interfacial energies [4], [5].

Shape-directed assembly is based on shape recognition between outline of components and receptor sites [6].

¹ National Science Foundation

² Micro-Electro-Mechanical Systems

³ Their work includes mainly surface tension driven Self-Assembly [1], [2], but also shape driven Self-Assembly in a wet environment [3].

1.2 Aim of the NSF 3D Self-Assembly project

The NSF project aims to investigate the fundamental principles of Self-Assembly processes; to build a science base and eliminate the ad hoc trial-and-error approach that is characteristic of current Self-Assembly.

The results of multiple experiments will let us elaborate *Self-Assembly models*, which will describe and predict the relationship between *system design parameters* (e.g., materials, geometry) and *process performance parameters* (e.g., assembly time, yield).

With these models, Self-Assembly systems can be designed in order to get an optimal process performance.

The experiments planned for the NSF project are based on dry three-dimensional shape directed Self-Assembly. Cube-shaped parts are introduced in a confined space on a shaking platform. Controlled agitation mixes the parts in a random fashion.

Cubes bind to each other when two adjacent surfaces come close to each other and their binding forces dominate the agitation forces.

2. APPROACH TO THE SELF-ASSEMBLY EXPERIMENTS

2.1 Design of the assembling components

The parts used for the experiments are produced on a silicon wafer with common methods of micro fabrication. Three different types of cubes are fabricated. Opposite sides of the cube have the same shape.

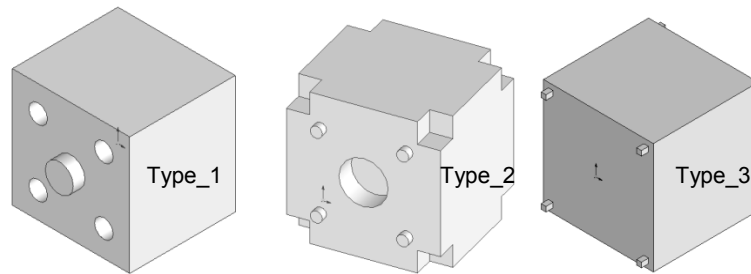


Figure 2: Design of the three different types of cubes

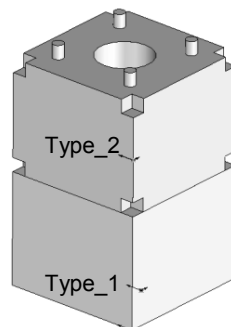


Figure 3: Assembly of a Type_1 and a Type_2 cube

Common micro fabrication methods allow us to only process the two surfaces of the wafer. The Type_3 can fit into the unprocessed sidewall of the Type_2 cubes as shown in Figure 4 to form a three-dimensional assembly structure.

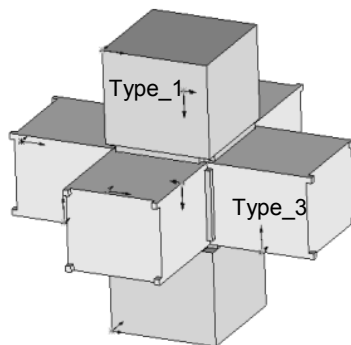


Figure 4: A three-dimensional assembly of Type_1, Type_2 and Type_3 cubes

The dimension length of a cube is $635 \mu\text{m}$ (0.025 inch).

To start the project, only Type_1 and Type_2 cubes are fabricated.

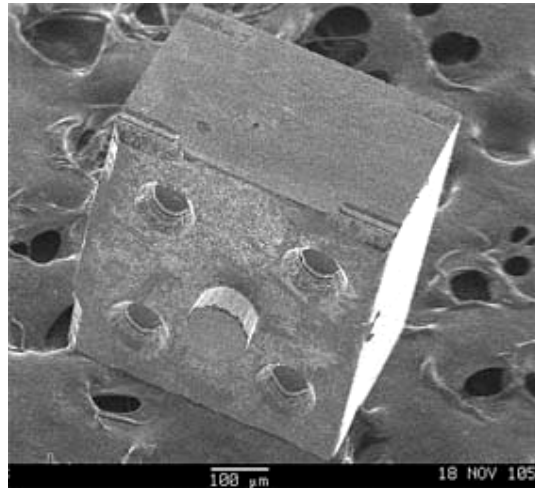


Figure 5: SEM picture of a Type_1 cube (background: carbon tape)

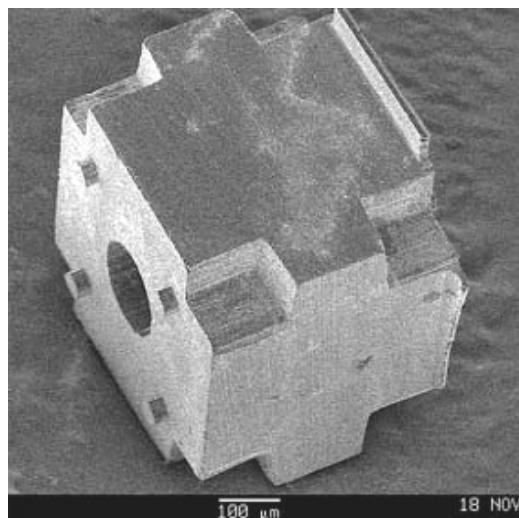


Figure 6: SEM picture of a Type_2 cube

About 1000 cubes of both types have been produced.

The cubes are inspected one by one under a microscope before being used in a Self-Assembly experiment to guarantee their conformity.

2.2 Design of the stage

The setup has a confined space in which the parts move randomly. The platform and the tube wall define the confined space (Figure 7). Random motion is provided by the platform, which is mounted on a vibrating stage.

To avoid the cubes sticking to the silicon stage, the surface of the stage is roughened up (Figure 9).

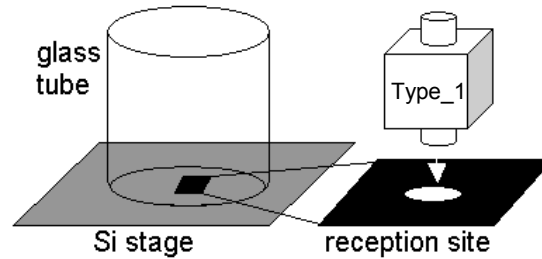


Figure 7: Silicon stage with a Type_1 reception site

The stage fabricated for the small setup, is designed with a Type_1 reception site in the center. In the first experiments, the cubes are supposed to assemble with each other and with the reception site on the stage.

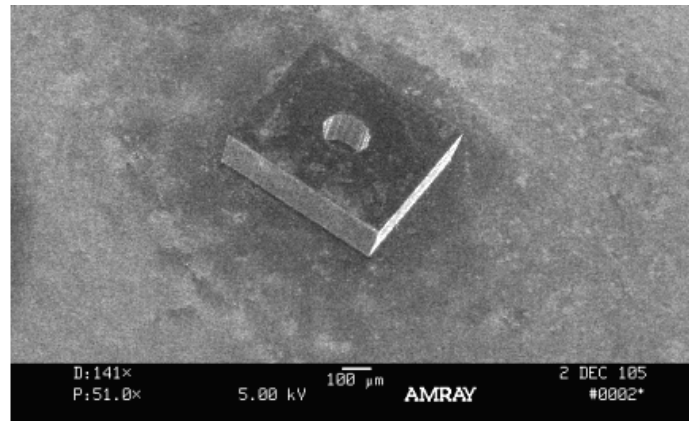


Figure 8: SEM picture of the reception site

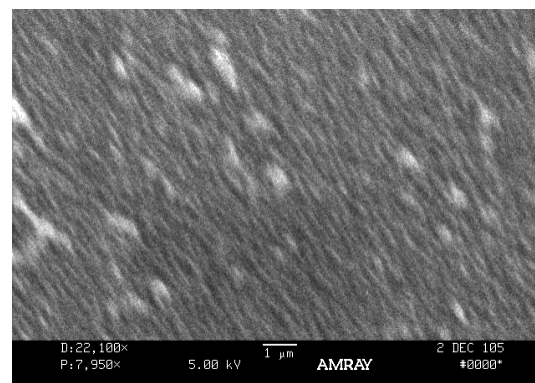


Figure 9: SEM picture of the rough silicon stage surface

2.3 Model of the Self-Assembly process

The *state of the system* consists of a vector $\vec{u} = \begin{pmatrix} u_1 \\ u_2 \\ \vdots \\ u_k \end{pmatrix}$

- u_i : number of assemblies of type i
- G_u : free energy assigned to the state u
- G_v : free energy assigned to the state v
- $k_{u,v}$: rate at which ~~the~~ state u transforms to v
- $k_{v,u}$: rate at which ~~the~~ state v transforms to u

The difference of the free energies from state u to state v ($G_u - G_v$) can be obtained by analyzing the physical binding forces between the cubes.

The Self-Assembly process is assumed to follow the *thermodynamic model* similar to that found in *chemical kinetics*. The relation between the rates $k_{u,v}$ and $k_{v,u}$ can thus be expressed with the following equation (2.2).

$$\ln\left(\frac{k_{v,u}}{k_{u,v}}\right) = \frac{-(G_u - G_v)}{E_T} \Leftrightarrow \frac{k_{v,u}}{k_{u,v}} = \exp\left(\frac{-(G_u - G_v)}{E_T}\right) \quad (2.2)$$

E_T is analogous to the thermal energy that is denoted $k_B T$ in a chemical reaction. ~~Where~~ k_B is ~~the~~ Boltzmann's constant and T is the temperature.

E_T is assumed to be proportional to the energy at which the system is agitated (Chapter 5.2).

3. DESIGN OF THE EXPERIMENTAL SETUP

A device is needed to provide a *controllable energy* to the cubes.

A ~~p~~ previous work with a similar assembly method has been done in the MEMS research group¹. The parameters used in this project give a rough idea about the required system parameters.

Shaking frequency: 10 - 300 Hz

Shaking amplitude: ~ 0.5 mm

We have three options:

- Use a device available in the laboratory
- Buy a device
- Design a device for this application

The required parameters are just a rough estimation. It is therefore not reasonable to design a device especially for this application.

3.1 Solution catalog and choice

Criteria for the solution choice:

- frequency range and displacement
- size
- complexity
- price

The following table summarizes three solutions.

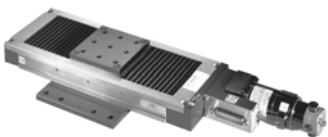
Name	Picture	Comment
Linear table		<ul style="list-style-type: none"> + good guidance + easy to work in closed loop + flexible usage - expensive - size
Woofers		<ul style="list-style-type: none"> + displacement big enough + high frequency range (0-200 Hz) - big size (50 x 50 x 80 cm)
Voice coil speaker		<ul style="list-style-type: none"> + easy to operate + compact, easy to move + cheap - weak guidance - difficult to do a closed loop control

Table 1: Solution catalog

¹ [2] Similar to this experiments, flat parts are agitated in a dry environment on a speaker. The parts bounce and assemble on a substrate placed above a speaker.

	Frequency	Displacement	Complexity	Size	Price
Linear Table	-	+	-	-	-
Woofers	+	+	+	-	-
Speaker	+	-	+	+	+

Table 2: Comparing the solutions

The capabilities of a linear table are much higher than the requirements. Only a small range of the possible displacement is needed for this application. Moreover, it is expensive. A cheaper, more adapted solution is thus preferable.

The woofer is already available in the lab and the system parameters fit for the application. One major disadvantage is the size of the woofer. It is a heavy device, which makes the setup less flexible.

The voice coil speaker is a cheap and compact device. A speaker can easily be moved around in the lab. This is important for the beginning of the experiments, as different devices in different locations in the lab are used.

The experimental setup for Self-Assembly experiment is therefore made with a *voice coil speaker*.

3.2 Speaker

The speaker used is based on a voice coil. The outer diameter of the cone is 4.5 inches.

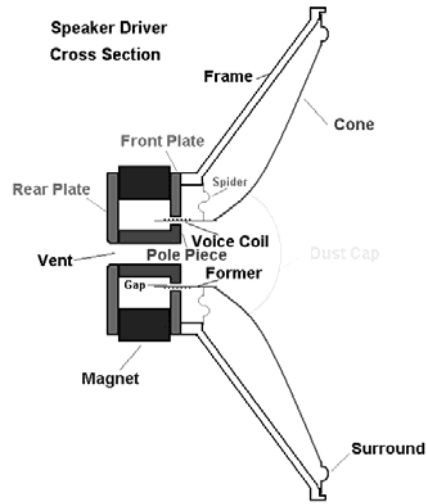


Figure 10: Schematic of a voice-coil speaker

The speaker's displacement can be expressed as a function of the voice coil input parameters: the frequency and the voltage. The law that links the parameters to the displacement is known as transfer function. The *mechanical model* of the speaker and the *electrical model* of the voice coil define the transfer function of a voice coil speaker.

3.2.1 Mechanical model

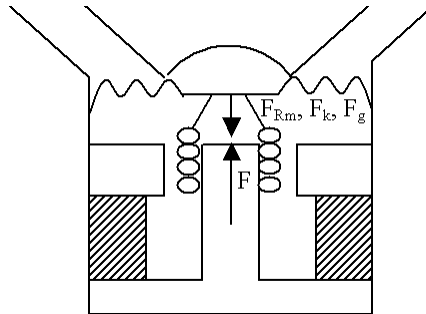


Figure 11: Forces acting on the speaker's cone

- b : mechanical damping coefficient
- k : mechanical stiffness
- B : magnetic flux density
- l : length of the voice-coil conductor immersed in the magnetic field
- i, L, R : voice-coil current, inductance and resistance
- z : position of the cone

To establish the mechanical model of a speaker, it is simplified to a system with a mass and the forces acting on the mass¹:

$$F = Bli \quad \text{force generated by the voice coil motor}$$

$$F_{Rm} = b\dot{z} \quad \text{mechanical damping force}$$

$$F_k = kz \quad \text{restoring force}$$

$$F_g = mg \quad \text{gravitational force}$$

$Z(t)$: displacement measured from the relaxed spring position

$z(t)$: displacement measured from static equilibrium position

Newton's law of motion can be written as follow:

$$m\ddot{Z} + b\dot{Z} + kZ + mg = Bli(t) \quad (3.1)$$

$$Z(t) = Z_0 + z(t) \quad (3.2)$$

$$m\ddot{z} + b\dot{z} + kZ_0 + kz(t) + mg = Bli(t) \quad (3.3)$$

$$\text{letting } t \text{ go to zero: } kZ_0 + mg = 0 \quad (3.4)$$

combine equations (3.3) and (3.4):

$$m\ddot{z} + b\dot{z} + kz(t) = Bli(t) \quad (3.5)$$

Laplace transformation of the equation (3.5):

$$mzs^2 + bzs + kz = Bli \quad (3.6)$$

3.2.2 Electrical model

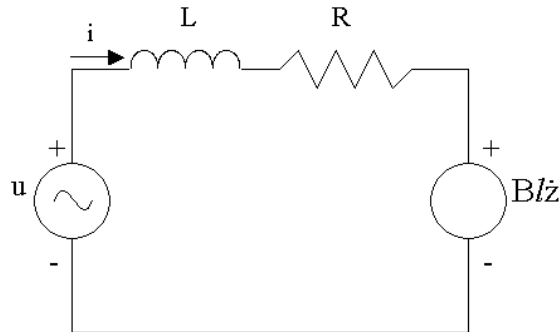


Figure 12: Scheme of the voice coil circuit

We can write the following equation using Kirchhoff's law:

$$u(t) = Bl\dot{z} + Ri + L \frac{di}{dt} \quad (3.7)$$

Laplace transformation of the equation (3.7):

$$U(s) = Blzs + Ri + Lis \quad (3.8)$$

¹ The mechanical model is established as proposed in [7]

3.2.3 Transfer function of the speaker

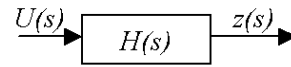


Figure 13: $H(s)$: Transfer function of the speaker

With the equations (3.6) and (3.8), the transfer function of the speaker can be expressed:

$$H(s) = \frac{z(s)}{U(s)} = \frac{Bl}{Lms^3 + (Lb + Rm)s^2 + (Rb + Lk + (Bl)^2)s + Rk} \quad (3.10)$$

The transfer function is a combination of an under-damped part with the cutoff pulsation ω_c and a pole with the cutoff pulsation ω_{c2} .

$$H(s) = \frac{z(s)}{U(s)} = \frac{K}{\left(\frac{1}{\omega_c^2}s^2 + 2\frac{1}{\omega_c}\xi s + 1\right) \cdot \left(\frac{1}{\omega_{c2}}s + 1\right)} \quad (3.11)$$

With equations (3.10) and (3.11), ω_{c2} can be expressed:

$$\omega_{c2} = \frac{Rk}{Lm\omega_c^2} \quad (3.12)$$

The specification of the speaker does not furnish the values of all the parameters. They are therefore estimated¹. ω_c is measured (Chap. 4.2.2): $\omega_c = 2\pi \cdot 18\text{Hz}$

$$\omega_{c2} = 3\text{kHz}$$

The pole with the cutoff pulsation ω_{c2} is not relevant in the frequency range the speaker is used ($\omega_{c2} > 1\text{kHz}$). Therefore the transfer function can be simplified to the following equation:

$$H(s) = \frac{z(s)}{U(s)} = \frac{K}{\frac{1}{\omega_c^2}s^2 + 2\frac{1}{\omega_c}\xi s + 1} \quad (3.13)$$

- K : gain
- ω_c : cutoff pulsation
- ξ : damping coefficient

K , ω_c and ξ are determined in chapter 4.

¹ Estimation of the speaker's parameters:
 $R = 8\Omega$, $k = 1.5\text{kN/m}$, $L = 1\text{mH}$, $m = 0.03\text{kg}$

3.3 Sensor research

Required functions of the sensor:

- provide data to calculate the kinetic energy of the shaker ($E_{kin} = \frac{1}{2}mv^2$)
- provide data to establish the shaking platform gain and phase, versus frequency
- easy assembly on the experimental setup

Criteria for the sensor choice:

- Performance of the sensor:
 - Bandwidth ($\sim 1\text{kHz}$)
 - Sensitivity
 - Measuring range ($\sim 5g^1$)
- Sensor mounting
- Price
- Size and weight (limited by the experimental setup)
- Availability (lead time < 3 weeks)

Possible sensor types:

- displacement sensor
- velocity sensor
- accelerometer

Displacement, velocity and acceleration are linked by derivation. The other two dimensions can therefore be acquired with every type of sensor mentioned above. However, these calculations generate errors, in particular when numerically integrating acceleration or velocity data to obtain position information.

¹ Approximate values of the speaker:

- amplitude: $A = 0.5 \text{ mm}$
- frequency: $f = 50 \text{ Hz}$

Assume that the speaker shakes in sine waves:

$$x = A \sin(\omega t)$$

$$v = \dot{x} = A \omega \cos(\omega t)$$

$$a = \ddot{x} = -A \omega^2 \sin(\omega t)$$

Maximum acceleration:

$$a_{max} = A \omega^2 = 0.5 \text{ mm} (2\pi \cdot 50 \text{ Hz})^2 = 49.3 \text{ m/s}^2 = 5.03g$$

Three suitable sensors are listed in the table below¹.

Type	Accelerometer	Accelerometer	Position sensor
Manufacturer	Analog devices	Silicon Designs, Inc	Baumer Electric
Product name	ADXL321EB	1210J-025	IWRM 08U9501/S35
Bandwidth (max)	2.5 kHz	1 kHz	1.4 kHz
Sensitivity	57 mV/g	160 mV/g	-
Dynamic resolution	-	-	5 μm
Measuring range	18 g	25 g	2 mm
Mounting	Screw EB on the Platform	Solder to the platform	Screw sensor on a fixed base
Price	30 \$	129 \$	163 \$
Size	20 x 20 mm	0.35 x 0.35 inch	∅ 6.5 x 46 mm
Lead time	1 week	1 week	2 weeks

Table 3: Summary of 3 sensors

All the sensors proposed in Table 3 fulfill the required sensor performances (bandwidth, sensitivity and measuring range).

	Prize	Size	Availability
ADXL321EB	+	+	+
1210J-025	-	-	+
IWRM 08U9501/S35	-	+	+

Table 4: Evaluation of the sensors

The ADXL321 Accelerometer is an adequate sensor for the measurements we need to do. It is a capacitive sensor, integrated in a chip that makes it small and easy to handle.

¹ The products are listed on the internet: [10], [11], [12]

3.4 Mechanical parts

The ADXL321 is a dual-axis accelerometer. In the experiment, one axis is relevant as the speaker moves just in one direction. The second degree of freedom can be used to indicate if the system moves properly in the z direction, or if there is a parasitic movement (4.2.1). The accelerometer is mounted upwards (Figure 14) to sense acceleration in the z direction.

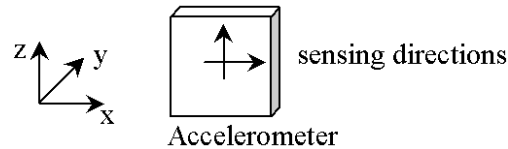


Figure 14: Sensing directions of the accelerometer

The setup consists of the following components:

- | | |
|----------------------|---------------------------|
| 1) Speaker | (Appendix V, Chapter 3.2) |
| 2) Plastic tube | (Appendix III) |
| 3) Aluminum platform | (Appendix III) |
| 4) Aluminum angle | (Appendix III) |
| 5) Accelerometer | (Appendix I) |
| 6) Silicon stage | (Chapter 2.2) |
| 7) Glass tube | (Appendix III) |

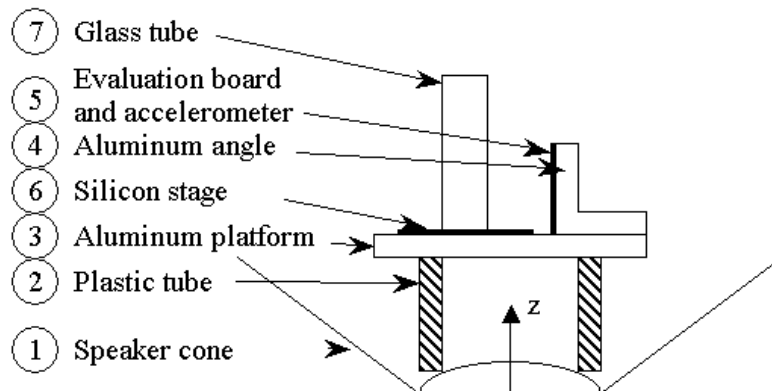


Figure 15: Assembly of the setup

Design constraints:

High eigenfrequency¹ of the mechanic part mounted on the speaker:

- high Young module of the material
- low mass

The first design of the setup was done with a small stage and a small glass tube. The first experiments were carried out with the small stage.

The Self-Assembly process is stochastic. The results are thus more significant, if the experiments are done with a large number of parts. Therefore, a second, bigger stage has been designed.

¹ The mechanical system is not supposed to be excited in a resonance frequency. The eigenfrequency of the mechanical system has to be higher than the shaking frequency.

3.5 Setup Assembly

The connections between the different components have to be rigid to transmit the movement of the speaker cone to the silicon stage without any loss of frequency bandwidth. There are different silicon stages used during the experiments. It is therefore important to make the silicon stage easily reconfigured.

All characterization measurements were conducted on the second setup (Figure 18).

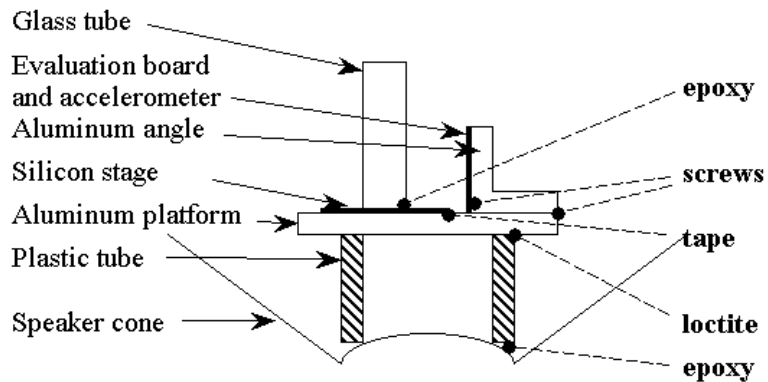


Figure 16: Scheme of the first setup assembly

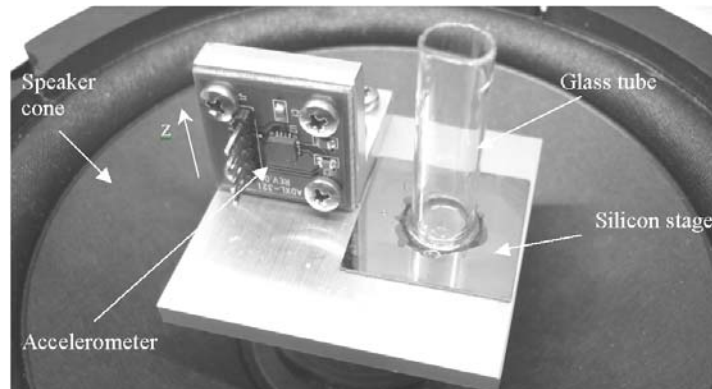


Figure 17: Small setup assembly

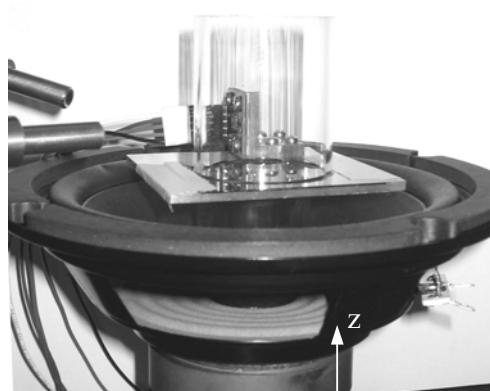


Figure 18: Final design with the large stage

4. SETUP CHARACTERIZATION

The aim of the characterization is to find the transfer function of the speaker and to predict the energy delivered to the assembling cubes by knowing the input parameters: frequency and amplitude.

4.1 Measuring arrangement

The measurements are carried out with the setup entirely assembled. A function generator provides the input signal for the speaker.

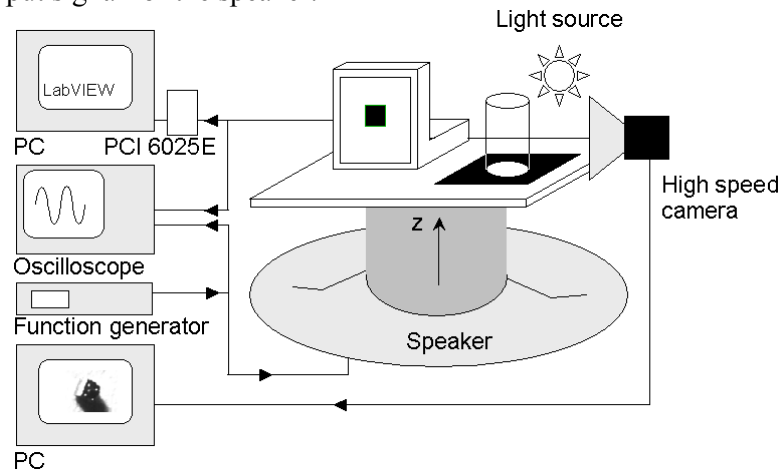


Figure 19: Measuring setup

4.1.1 Accelerometer calibration

The accelerometer output is a voltage.

To calibrate the sensor, the acceleration is measured in the x and z direction. In the z direction, earth gravitation is sensed, but not in x . The difference between the two signals corresponds consequently to g .

These measurements are done on the static system (no excitation of the speaker) and with an accelerometer supply voltage of 3.5V, which is maintained during the measurements.

$x_{Acc Output}$: 1.752 V

$z_{Acc Output}$: 1.672 V

g corresponds to 0.08 V

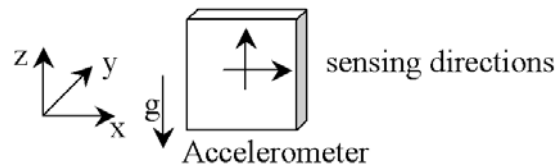


Figure 20: Orientation of the accelerometer

V_A : voltage [V]

A : acceleration [m/s^2]

$$A = \frac{V_A}{0.08} \cdot 9.81 \quad (4.1)$$

4.1.2 Calculation of the displacement

The displacement measurement is generated in two different ways.

With the assumption that the displacement is sinusoidal, it can be calculated as follows:

$$z_{max} = \frac{a_{max}}{(2\pi f)^2} \quad (4.2)$$

The observed acceleration is sinusoidal for input amplitudes from 1 to 5V. At higher amplitudes, there is a second harmonic superimposed on frequencies below 20 Hz.

The second way to get the displacement amplitude is to double-integrate the signal of the accelerometer. This is done using LabVIEW. The accelerometer signal output is converted into a digital signal with a PCI card¹.

The plots and the calculation of the displacement are done with the following parameters:

$$V = 6 \text{ V}$$

$$f = 18 \text{ Hz}$$

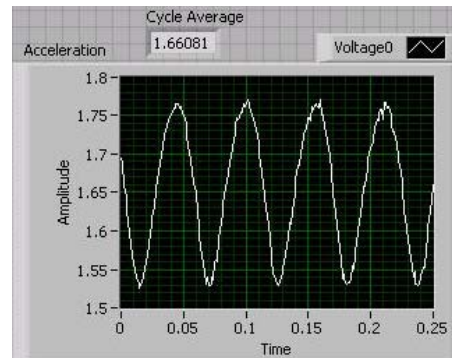


Figure 21: Acceleration

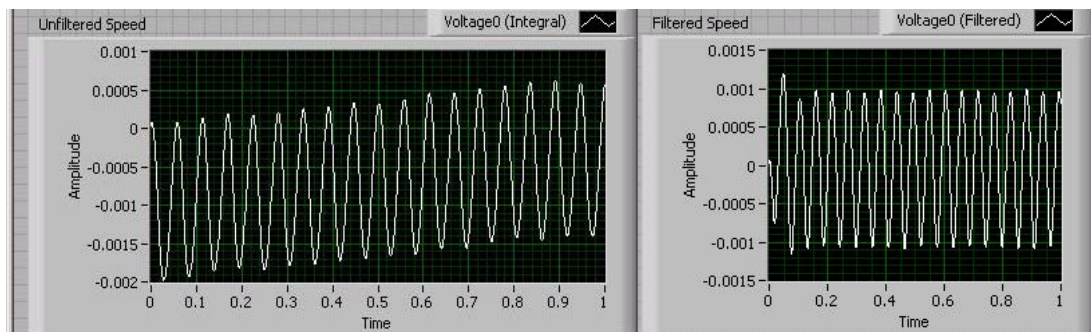


Figure 22: Unfiltered and filtered Speed

The accelerometer output varies around a nonzero bias voltage. This voltage changes slightly during the measurement and makes the integrated curve drift. The drift can be eliminated with a high pass filter. The cutoff frequency of the filter must be adapted to the shaking frequency.

¹ NIDAQ 6025E [13]

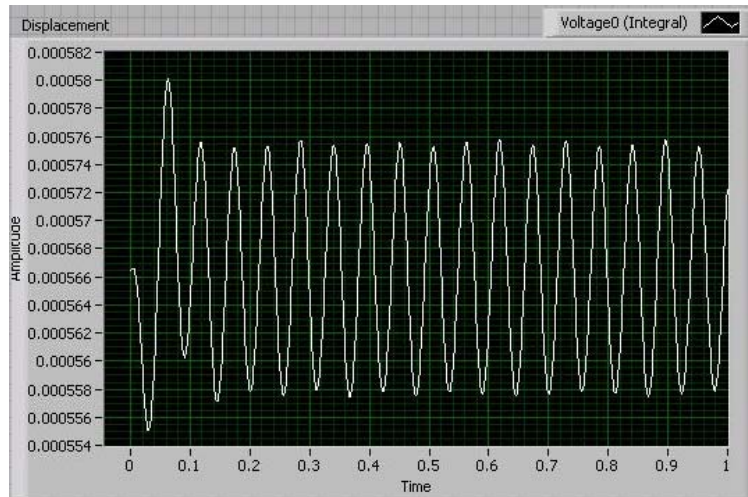


Figure 23: Displacement

The value of the displacement (ΔV_z) can now be taken from the plot (Figure 23) and converted into a metric displacement with equation (4.1).

$$\Delta V_z = 18 \cdot 10^{-6} \text{ V}$$

$$\Delta z = \frac{\Delta V_z \cdot 9.81}{0.08} = 2.2 \text{ mm}$$

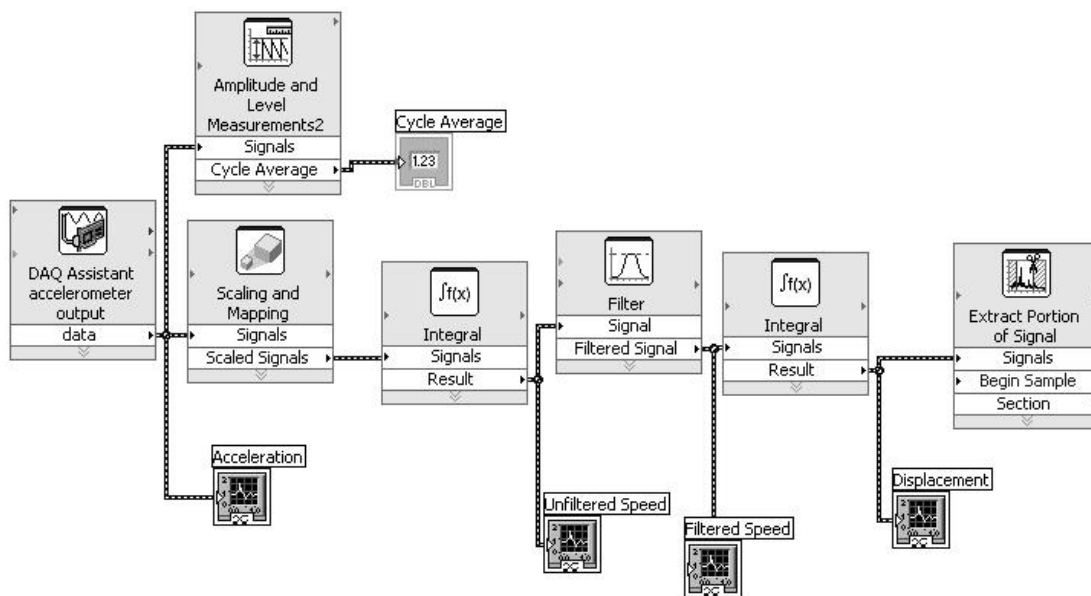


Figure 24: LabVIEW Block diagram

The first way to get the displacement is preferable, because there are no errors from the numerical double-integration in the result.

4.1.3 Comments on the measuring setup

The function generator does not provide enough current to keep the input voltage of the speaker at a constant value. The speaker load pulls the voltage down.

V_{F_out} : Output voltage of the function generator
 V_{S_in} : Speaker input voltage

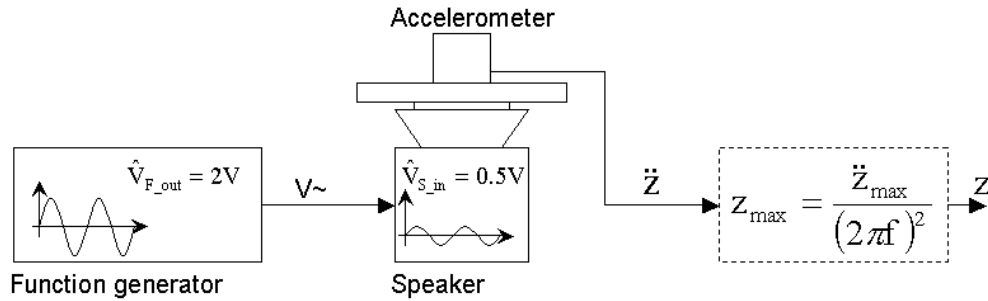


Figure 25: Example of the voltage reduction due to the speaker load at 18 Hz

The drop of the speaker input voltage is not constant for different frequencies.

Two transfer functions can now be established, one to characterize the shaker:

$$z_{max} / V_{S_in} \quad (z_{max} = \text{Amplitude of the displacement})$$

The second transfer function describes the whole system, which includes the function generator:

$$z_{max} / V_{F_out}$$

The first model corresponds to the theoretical model established in chapter (3.1). The second system is more useful for the practical experiments, because it describes the displacement as a function of the amplitude setting of the function generator.

The measurement were carried out on a non-vibration isolated table.

Plot 1 and 2 (Appendix I) show the accelerometer output while the shaker is not vibrating. The amplitude of the noise is similar in both cases. The measured signals are 100 times bigger than the noise signal; the noise is thus not influencing the results of the measurements.

For the establishment of the gain and phase of the platform, the speaker input amplitude is set to a constant voltage V while the frequency is varied from 5 Hz to 1 kHz.

The bandwidth of 1 kHz is set with a capacitor on the sensor evaluation board. This SMD capacitor is soldered on the evaluation board and not changed for the different measurements. This implies that on the lower frequencies, the measured signal has more noise and the measurements at the lower frequencies (<50 Hz) are therefore less accurate.

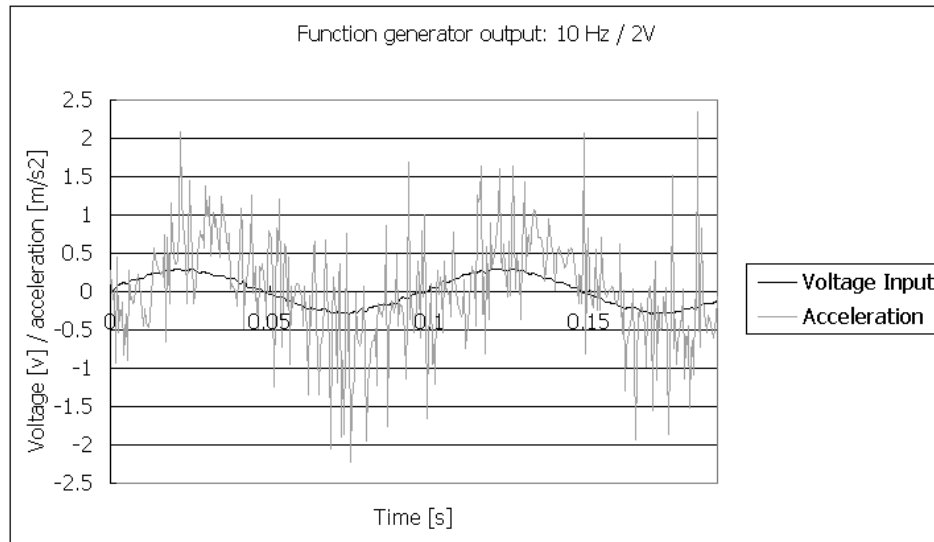


Figure 26: Speaker input and accelerometer output at 10 Hz

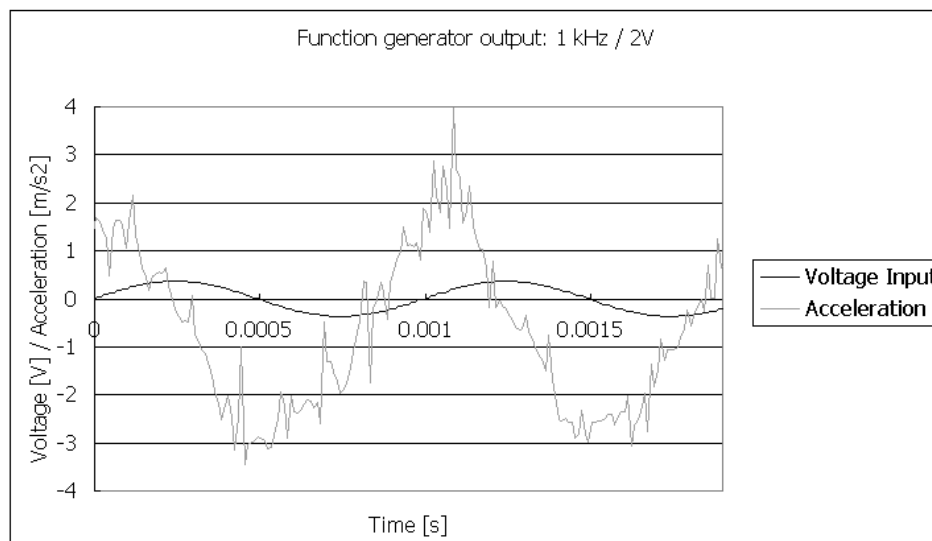


Figure 27: Speaker input and accelerometer output at 1 kHz

4.2 Results

4.2.1 Analysis of the shaking direction

Calculation of the center of gravity:

$$\rho_{Al} = 2700 \text{ kg/m}^3, \rho_{Glass} = 2320 \text{ kg/m}^3$$

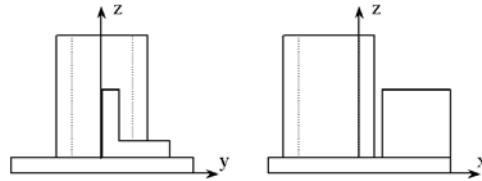


Figure 28: Disposition of the mechanical components on the speaker in the yz- and xz-plane

	<i>i</i>	Volume [$\cdot 10^{-6} \text{m}^3$]	Mass [g]	x_i	y_i
Aluminum platform	1	22.5	60.8	0	0
Aluminum angle	2	5.16	13.9	25.5	7.8
Glass tube	3	14.7	34.1	-12	0
Σ			108.8		

Table 5: Center of gravity of the different components

$$x_s = \frac{\sum_i (x_{s,i} \cdot m_i)}{\sum_i m_i} = \frac{0 \cdot 60.8 + 25.5 \cdot 13.9 - 12 \cdot 34.1}{108.8} = -0.5 \text{ mm}$$

$$y_s = \frac{\sum_i (y_{s,i} \cdot m_i)}{\sum_i m_i} = \frac{0 \cdot 60.8 + 7.8 \cdot 13.9 + 0 \cdot 34.1}{108.8} = 1 \text{ mm}$$

The center of gravity is still inside of the voice coil, but it is not exactly in the center. The lateral movement, which is generated that way, is shown in Figure 29.

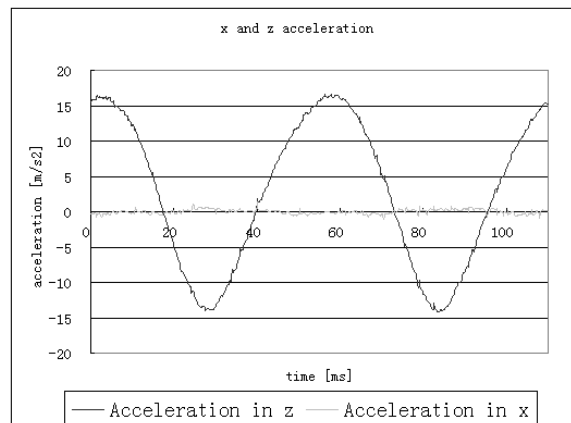


Figure 29: Measured acceleration in x and z-direction

The x and z direction corresponds to the directions indicated in Figure 28. The amplitude of the acceleration in x is small: $|\ddot{x}_{max}| \cong 1 \text{ m/s}^2$

It can therefore be neglected for the characterization of the setup.

4.2.2 Characterization of the shaker

The first Bode plot describes just the characteristics of the shaker. The magnitude corresponds to the displacement divided by the speaker input voltage z_{max}/V_{s_in} . This Bode plot fits the model established in chapter 3, equation (3.13).

$$H(s) = \frac{z(s)}{U(s)} = \frac{K}{\frac{I}{\omega_c^2} s^2 + 2 \frac{I}{\omega_c} \xi s + I}$$

A graphical curve fitting has been done to determine the parameters K , ω_c and ξ .

These measurements were carried out with the following parameters:

Function generator output voltage: 2 V
 Accelerometer input voltage: 3.5 V

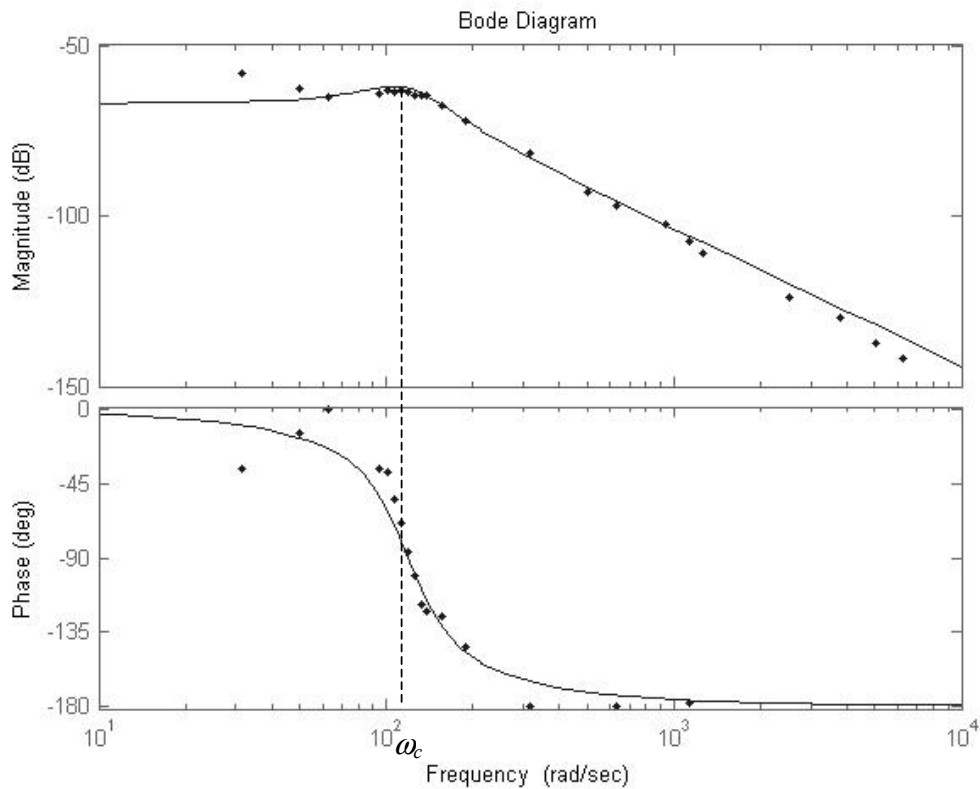


Figure 30: dots: measured values, line: model of the transfer function

$$\xi = 0.3$$

$$\omega_c = f_c \cdot 2 \cdot \pi = 19.2 \cdot \pi = 119 \text{ rad/s}$$

$$K = 4.47 \cdot 10^{-4}$$

$$H(s) = \frac{z(s)}{U(s)} = \frac{4.47 \cdot 10^{-4}}{7.02 \cdot 10^{-5} s^2 + 5.03 \cdot 10^{-3} s + 1} \quad (4.1)$$

4.2.3 Characterization of the entire system

The magnitude corresponds to the displacement divided by the function generator output voltage z_{max} / V_{F_out} .

These measurements were carried out with the following parameters:

Function generator output voltage: 2V

Accelerometer input voltage: 3.5 V

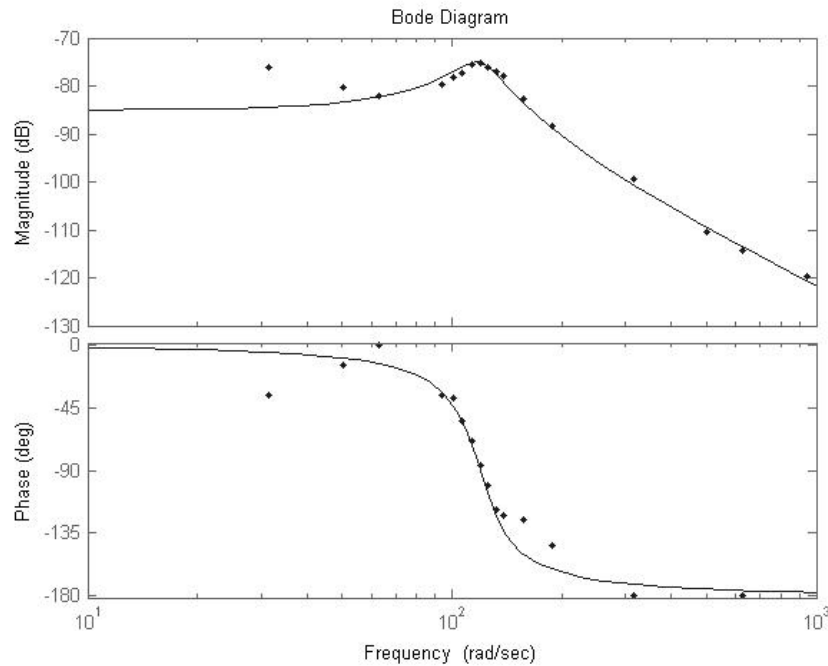


Figure 31: Bode diagram, dots: measured values, line: model of the transfer function

$$\xi = 0.16$$

$$\omega_c = f_c \cdot 2 \cdot \pi = 19 \cdot 2 \cdot \pi = 119 \text{ rad/s}$$

$$K = 5.62 \cdot 10^{-5}$$

$$H(s) = \frac{z(s)}{U(s)} = \frac{5.62 \cdot 10^{-5}}{7.02 \cdot 10^{-5} s^2 + 2.68 \cdot 10^{-3} s + 1} \quad (4.2)$$

The cutoff frequency of the entire system is at 19 Hz.

The acceleration increases constantly with the applied voltage (Figure 32). Equation (4.2) is thus valid for different voltages.

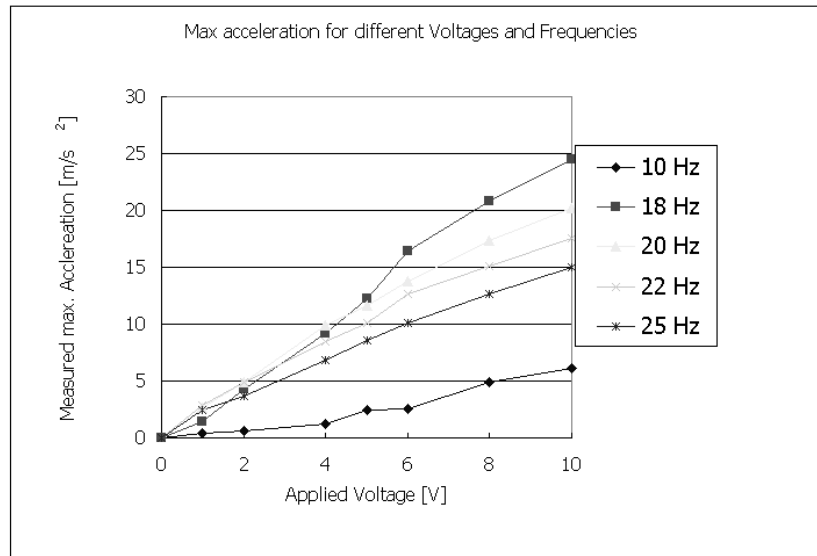


Figure 32: Maximum acceleration as a function of the function generator output voltage

4.2.4 Conversion: Function generator to displacement

Expressing the modulus of the complex transfer function (equation 4.2)), equation (4.3) is obtained. The equation (4.3) links the frequency and the voltage (set on the function generator) to the displacement of the speaker.

$$z_{max} = U \cdot \sqrt{\frac{3.16 \cdot 10^{-9} - 1.66 \cdot 10^{-11} f^2 + 2.43 \cdot 10^{-14} f^4}{1 - 5.26 \cdot 10^{-3} f^2 + 7.68 \cdot 10^{-6} f^4}} \quad (4.3)$$

The following plot shows the displacement of the speaker, with the function generator output voltage at 2V. The equation (4.2) is thus a valid model for this system.

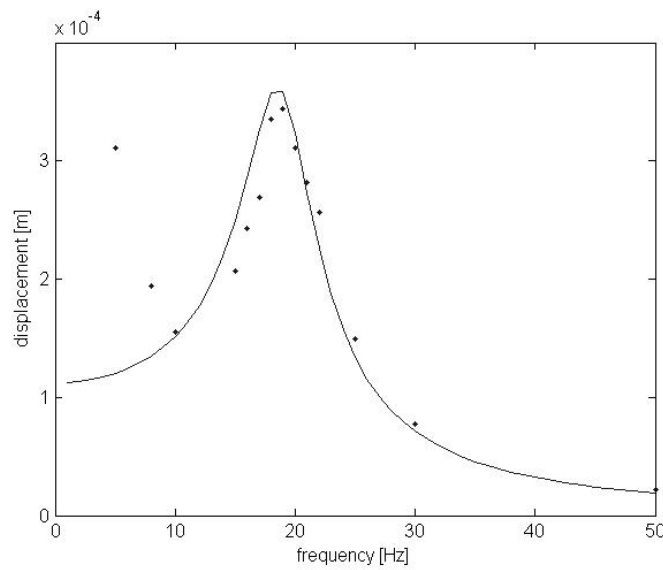


Figure 33: Displacement at $V_{F_out} = 2V$, dots: measured displacement, curve: equation 4.3

Below 10 Hz, the measured values differ from the theoretical curve. This is due to measurement errors. At low frequencies, the accelerometer output has a high noise (Figure 26).

4.3 Energy model

The kinetic energy provided by the platform is known:

$$E_{kin} = \frac{1}{2} m_{shaker} (v(t))^2 = \frac{1}{2} m_{shaker} (z_{max} \omega)^2 \cos^2(\omega t)$$

It is now interesting to know the energy of one cube for the generation of the assembly model.

4.3.1 Simulation

First, the energy of one part is obtained by simulating a bouncing mass point on a platform with a sinusoidal displacement on Matlab (Appendix IV).

The system specific parameters for the simulation are:

- $m1$: mass of a cube
- $m2$: mass of the moving platform
- $v1$: initial velocity of the cube
- $v1_{new}$: velocity of the cube after the impact
- $v2$: initial velocity of the platform
- $v2_{new}$: velocity of the platform after the impact
- α : coefficient of restitution
- $A2$: shaking amplitude (corresponding to the frequency and the applied voltage)
- f : shaking frequency

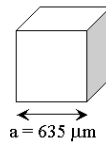


Figure 34: dimension length of a cube

$$m1 = V_{cube} \cdot \rho_{Si} = (635 \mu m)^3 \cdot 2330 \text{ kg/m}^3 = 0.597 \mu g$$

$$m2 \gg m1$$

inelastic impact:

$$v1_{new} = v2 + \alpha(v2 - v1)$$

$$v2_{new} = v2$$

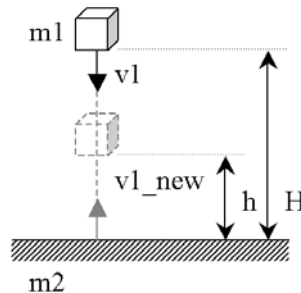


Figure 35: Inelastic impact between a cube and the shaking platform

$$\alpha = \frac{h}{H}$$

$$f = 18 \text{ Hz}$$

$$V = 6 \text{ V}$$

$$A2 = 1.29 \text{ mm}$$

The coefficient of restitution quantifies the energy, which is absorbed by the impact (i.e. transformed into thermal energy, deformation, or noise). α is found experimentally by dropping a cube down on the silicon stage and measuring the bouncing height¹:

$$\alpha = 0.34 \pm 0.2$$

To keep the model manageable, following assumptions have been done:

- α includes all the physical phenomena appearing at the impact of the cube:
 - elastic deformation of the cube and the stage
 - surface forces
 - geometry of the cube
- α is constant for different bouncing heights

The first plot in Figure 36 shows the sinusoidal displacement of the speaker surface and above the sinusoidal curve, the trajectory of the bouncing cube. With this set of parameters, the cube is in a repetitive cycle; it follows the upwards direction on the surface of the speaker and only gets in flight, when the speaker changes its direction.

The second plot shows the total energy of one cube, which is the sum of the potential and kinetic energy. The total energy of a cube stays constant in flight and it abruptly drops at an impact.

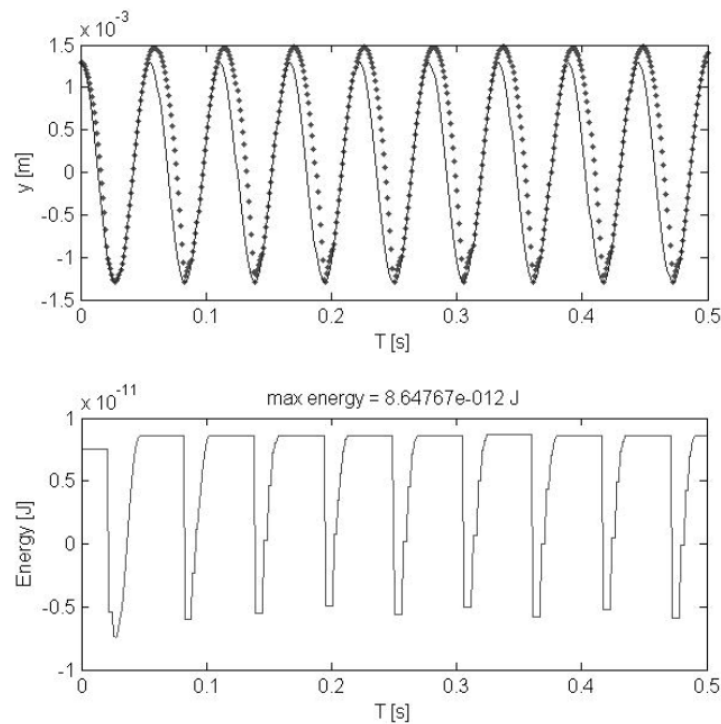


Figure 36: Results of the Matlab simulation

The simulated model assumes a point object. In reality, the objects are cubes.

¹ Simulation results for different values of α :

α :	0.32	0.34	0.36
$E_{cube,max}$:	$8.63 \cdot 10^{-12}$ J	$8.65 \cdot 10^{-12}$ J	$8.75 \cdot 10^{-12}$ J

Simulation with another set of parameters:

$\alpha = 0.36$
 $V = 8 \text{ V}$
 $f = 19 \text{ Hz}$
 $A_2 = 1.33 \text{ mm}$

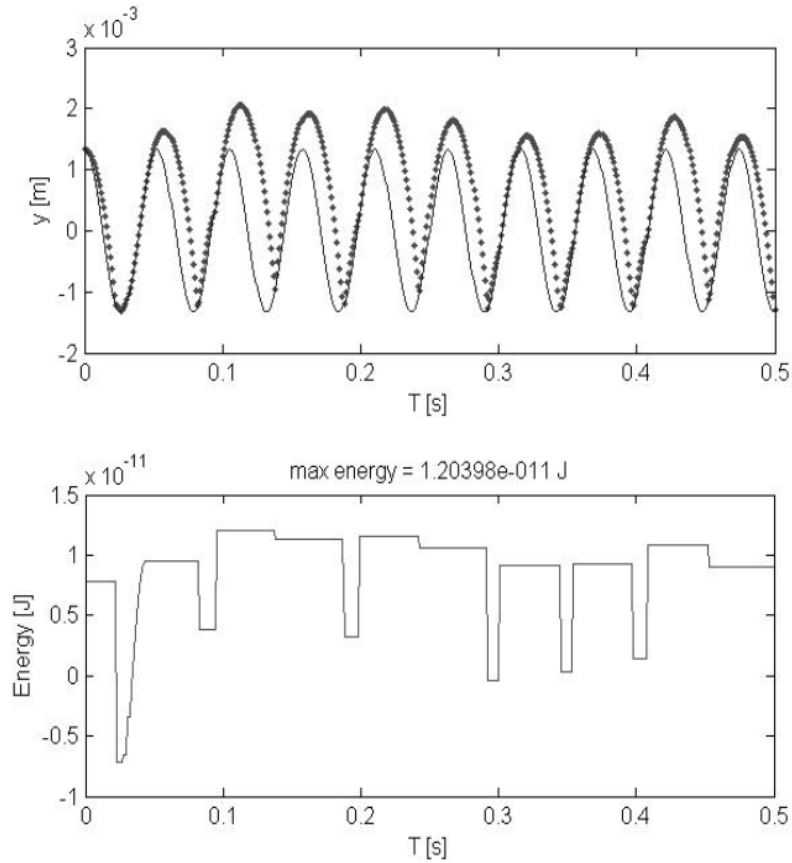


Figure 37: non regular movement of a cube

In this case, the cube is not in the same frequency as the speaker movement and the bouncing of the cube is not in the same regular mode as before.

4.3.2 Measurement

For a precise measurement of the energy, complex systems would be necessary¹. To get an approximation of the energy, a video has been taken of the shaking parts and the highest part positions have been traced (5.1.2).

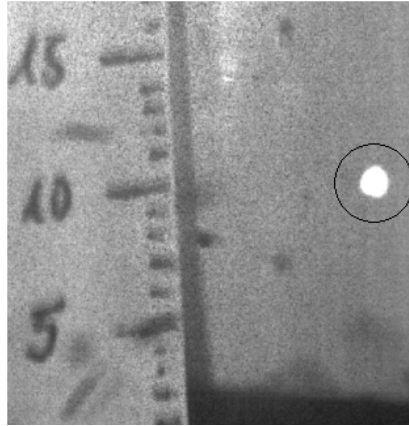


Figure 38: Height measurement of an agitated cube

$$h_{max} = 10 \pm 1 \text{ mm}$$

$$E_{cube, max} = m l \cdot g \cdot h_{max} = 5.86 \pm 0.6 \cdot 10^{-11} \text{ J}$$

Considering a cube spinning at a speed of $\omega = 100 \text{ rad/s}$, the kinetic rotational energy can be calculated:

$$E_{kin, rotation} = \frac{1}{2} I \omega^2 = \frac{1}{12} m_c a^2 \omega^2 = 2 \cdot 10^{-13} \text{ J}$$

The kinetic rotation energy is negligible compared to the potential energy.

4.3.3 Evaluation

	<i>Matlab simulation</i>	<i>Measured Energy</i>
$E_{cube, max}$	$0.87 \cdot 10^{-11} \text{ J}$	$5.86 \cdot 10^{-11} \text{ J}$
Comments	<ul style="list-style-type: none"> ▪ The cubes are considered to be spherical: in reality, the part can get a non vertical velocity component because of the cubic shape ▪ Measurement errors (in α) ▪ Numerical errors can appear in the simulation, due to rounding 	<ul style="list-style-type: none"> ▪ Measurement errors (in the height measurement)

Table 6: Comparison between the simulation and the measurement

Different bouncing modes are observed in the simulation. In reality, the parts ~~won't~~ stay in one mode. One reason for this is the non-spherical shape.

The measured energy is about 7 times higher than the simulated energy.

The simulated result is too low; one reason can be that the value for α used in the simulation is too low.

¹ In a previous work [8] an attempt has been done to trace the kinetic energy of one silicon component over time.

5. RESULTS OF THE EXPERIMENTS

5.1 Observations

5.1.1 Experiments done with the small stage

The first cycle of experiments has been carried out on the small setup. The purpose of the first experiments was to observe the behavior of the cubes on the shaking platform and to take a decision on how to proceed.

None of the cubes assembled on the reception site (Figure 8), however we could observe a Type_1 cube assemble with a Type_2 cube, with the following parameters:

Amplitude: 6 V

Frequency: 25 Hz

The surface of the small setup is 78.5 mm^2 . 6 cubes are placed in the tube.

The results of the experiments get more significant with a higher number of cubes, because of the stochastic behavior of the Self-Assembly process. This is the reason for the design of the bigger stage, on which the further experiments have been carried out.

5.1.2 Experiments done with the big stage

The experiments are done with a part density of 8 cubes per cm^2 :

$$\text{Surface in the glass tube: } S = \pi \cdot (2\text{cm})^2 = 12.57 \text{ cm}^2$$

50 cubes of each type are needed.

The maximum height of the bouncing cubes is measured for the different amplitudes and frequencies. The measurement is based on pictures, taken with a high-speed camera. The frame rate is set on 100 f/s, 30 frames are analyzed.

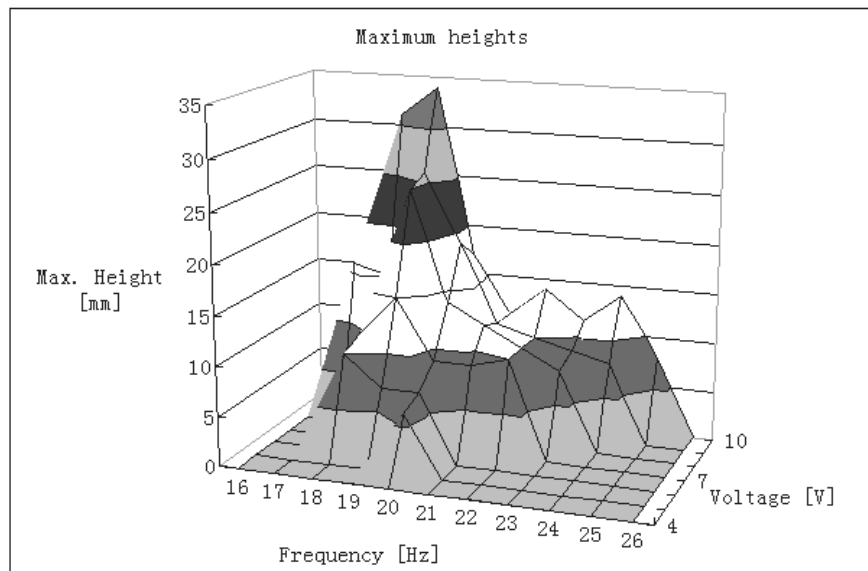


Figure 39: Maximum bouncing height of the agitated cubes

The maximum height is observed at a frequency of 19 Hz, which corresponds to the cutoff frequency of the setup.

The maximum kinetic energy provided by the shaker¹ can now be compared to the maximum kinetic energy of a cube (E_{cube}). Below a threshold value of the kinetic energy of the shaker, the cubes just follow the movement of the speaker and don't bounce:

$$E_{cube, threshold} = 35 \text{ nJ}$$

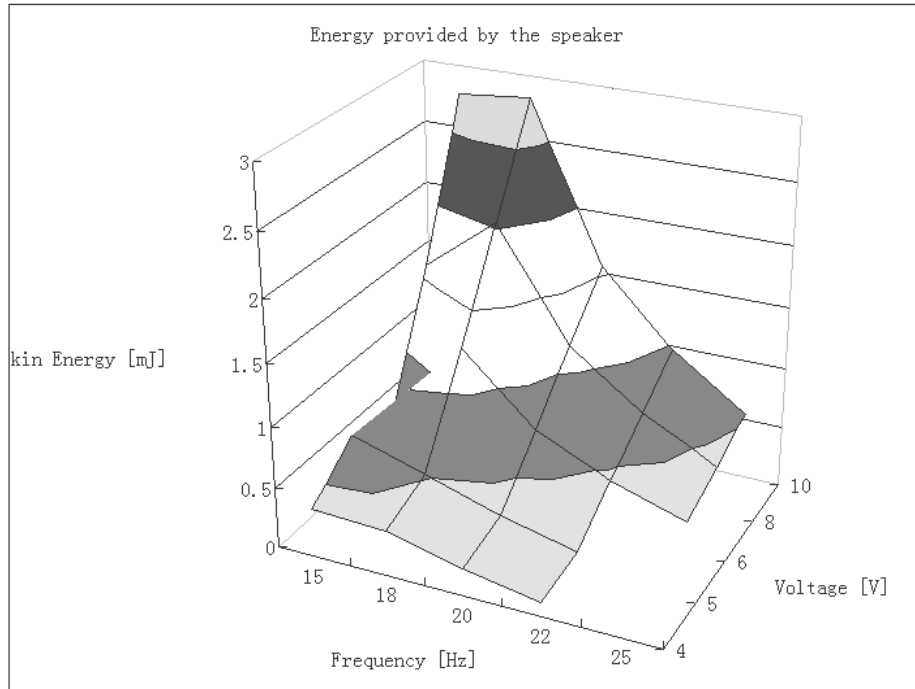


Figure 40: Maximum kinetic energy of the speaker

The measured maximum potential energy of the cubes is not exactly proportional to the kinetic energy provided by the speaker.

When the cube is bouncing, the average value of the relationship between the two energies (η_{bounce}) is:

$$\eta_{bounce} = E_{cube} / E_{kin} = 6,6 \cdot 10^{-8}$$

This is roughly 10 times bigger, than when the cube just follow the movement of the shaker².

During the experiments, no assembly could be observed.

Either, the cubes simply do not assemble or they assemble and release, because of a too small difference between G_u and G_v , equation (2.2).

¹ $E_{shaker} = \frac{1}{2} m_2 \cdot v^2$; with $m_2 = 0.12 \text{ kg}$

² The cube follows the movement of the shaker: $E_{cube} = \eta E_{shaker}$; $\eta = \frac{m_1}{m_2} = 5 \cdot 10^{-9}$

5.2 Identification of the model parameters

The analog value to thermal energy, E_T is assumed to be proportional to the energy at which the system is agitated:

$$E_T = C \cdot E_{kin}$$

Where C is a constant.

Equation (2.2) can be written as follow:

$$\frac{k_{v,u}}{k_{u,v}} = \exp\left(\frac{-(G_u - G_v)}{C \cdot E_{kin}}\right) \quad (5.1)$$

The difference of the free energies $G_u - G_v$ can be evaluated by analyzing the physical forces between the cubes.

The experiments are done as follows:

The cubes are shaken for a certain time Δt . Then, the shaking is stopped and the number of the different assembly types u_i is counted.

Time $t = n \cdot \Delta t$			
i	Assembly	Number of cubes	u_i^n
1	Single Type_1 cubes	1	
2	Single Type_2 cubes	1	
3	Type_1 and Type_2 assembled	2	
4	Two Type_1 and one Type_2	3	
5	Two Type_2 and one Type_1	3	
...			

Table 7: Table template for the experiments

After counting the assemblies, the stage is agitated for another time Δt and the counting process is repeated. The number of each assembly type is tracked over time.

The counted number of the assembly types define the vectors u^1, u^2, \dots, u^n representing the count of all possible assembly configurations.

Analyzing the reaction where two single parts assemble:

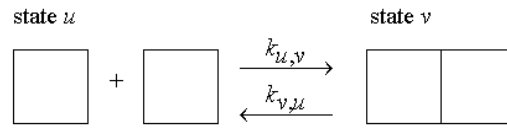


Figure 41: A Type_1 cube and a Type_2 cube assemble

m: number of unbound cubes ($u_1 = u_2 = m/2$)

At the beginning, the state of the system corresponds to vector u^0 . After n time intervals Δt , the state of the system is represented with the vector u^n .

$$\bar{u}^0 = \begin{pmatrix} u_1^0 \\ u_2^0 \\ u_3^0 \\ \vdots \\ u_k^0 \end{pmatrix} = \begin{pmatrix} m/2 \\ m/2 \\ 0 \\ \vdots \\ 0 \end{pmatrix} \quad \bar{u}^1 = \begin{pmatrix} u_1^1 \\ u_2^1 \\ u_3^1 \\ u_4^1 \\ \vdots \\ u_k^1 \end{pmatrix} = \begin{pmatrix} m/2 - 1 \\ m/2 - 1 \\ 1 \\ 0 \\ \vdots \\ 0 \end{pmatrix} \quad \dots$$

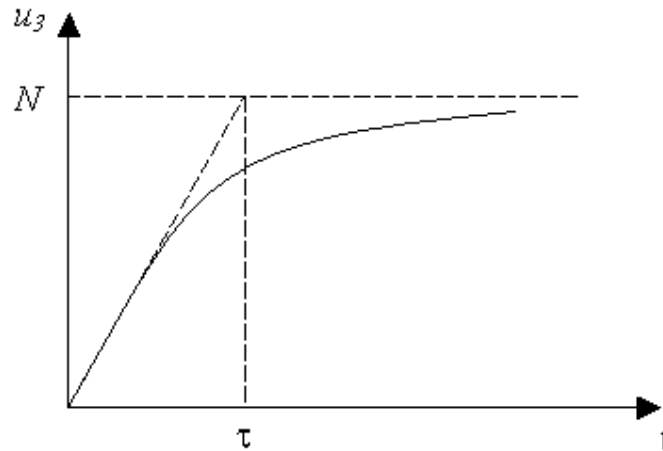


Figure 42: expected curve for assembly type u_3

N : maximal number of assemblies u_3

$$u_3(t) = N(1 - e^{-t/\tau}) \quad (5.2)$$

$$t = n \cdot \Delta t$$

τ is directly identified by the graph (Figure 42).

Taking the measuring results at different time intervals **n**, the parameters $k_{u,v}$ and $k_{v,u}$ can be calculated.

$$u_3^n = N(1 - e^{-n\Delta t/\tau}) = u_1^{n-1} u_2^{n-1} \cdot \Delta t \cdot k_{u,v} + u_3^{n-1} (1 - \Delta t \cdot k_{v,u}) \quad (5.3)$$

Once the parameters $k_{u,v}$ and $k_{v,u}$ are identified experimentally, they can be replaced in equation (5.1) and the assumption for the chemical analogy can be evaluated.

5.3 Part density

The part density can be measured for a certain height, with a high-speed camera:
 The camera is mounted on the top of the speaker and faces down in the z direction. The *depth of focus* of the camera defines the range¹, in which the parts are counted. Adapting the depth of focus on different heights, it is possible to count the number of sharp cubes for a certain height and a certain instant in time. With a small depth of focus, smaller height ranges can be measured and thus, more measure points will be obtained.

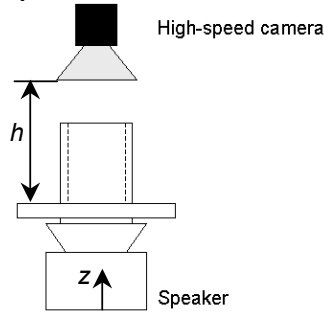


Figure 43: Setup for the part density measures

Camera settings:

- Height h : 230 mm
- Aperture: 2.8
- Recorded frame rate: 25 frames/s
- Shutter speed: 1/25 s

100 cubes are agitated at a frequency of 18 Hz and amplitudes from 6 to 8V. The cubes, which are sharp in the image, are counted in 10 consecutive frames, the y-axis of the plot indicates the number of cubes observed at the specific height during 2,5 seconds.

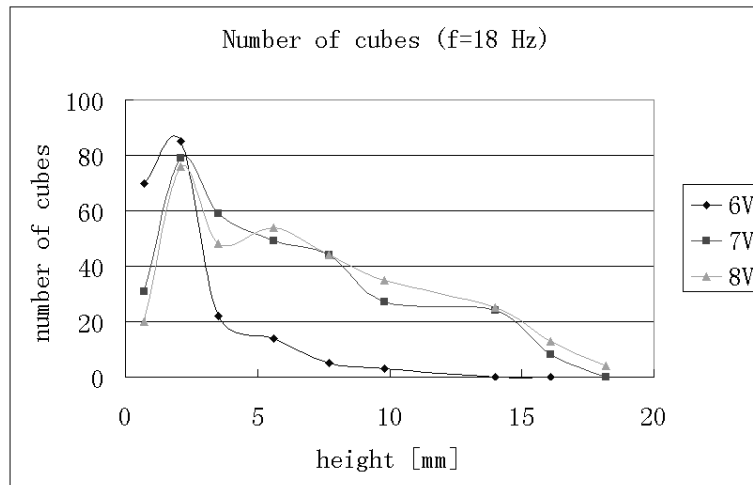


Figure 44: Cube density at different heights

These curves on the graph provide information about the kinetic energy of the cubes at different heights. They also show the cube density at different heights, which can be interpreted as pressure.

¹ The depth of focus changes with the aperture of the lens. With a small aperture, a big depth of focus is obtained.

6. CONCLUSION

The experimental setup is suitable for what is needed at this point:

- The setup is compact and light and it can easily be moved to different places.
- The *cutoff frequency* is at 19 Hz. It is very low and restricts the frequency range in which the experiments can be done.
- Below the cutoff frequency, the *displacement* of the platform is adequate.
- The *design* of the setup allows taking the stage off the platform and put it under a microscope, this makes the part counting convenient.
- The accelerometer is a good solution for the *sensor* choice. Its performance fits the requirements. One disadvantage of the accelerometer is that the capacitance that defines the bandwidth is a SMD component, which makes it difficult to adapt the bandwidth.

The low cutoff frequency is a disadvantage of the setup. It could be interesting to use the woofer available in the lab to observe the shaking of the cubes at higher frequencies.

The Self-Assembly experiments are not successful. On the experiments with the big stage, no assembly could be observed.

The fact that the cubes do not assemble reflects that the difference of free energy from state u to state v is positive or close to zero (2.2) and thus: $k_{u,v} \leq k_{v,u}$.

The results of the experiments show; that the cubes stick to the silicon surface when the shaker provides little energy. Increasing the energy, the cubes start to bounce freely and their energy is too high, to assemble with other cubes.

For further experiments, it is thus important; to analyze these binding forces. The system should be designed in a way, that the force that makes two cubes stick to each other is much higher than the binding force between a cube and the substrate.

7. REFERENCES

- [1] X. Xiong, Y. Hanein, J. Fan, Y. Wang, W. Wang, D. T. Schwartz, K. F. Böhringer, “Controlled Multibatch Self-Assembly of Microdevices”, *Journal of Microelectromechanical systems*, Vol. 12, April 2003
- [2] Sheng-Hsiung Liang, Kerwin Wang, K. F. Böhringer, “Self-Assembly of MEMS Components in Air Assisted by Diaphragm Agitation”, *IEEE Conference on Microelectromechanical systems (MEMS)*, January 2005
- [3] J. Fang, S. Liang, K. Wang, X Xiong, K.F. Böhringer, “Self-Assembly of Flat Micro Components by Capillary Forces and Shape Recognition”, 2nd annual Conference on Foundations of Nanoscience: Selfassembled Architectures and Devices (FNANO), Snowbird, UT, April 24-28, 2005
- [4] Richard R. A. Syms, Eric M. Yeatman, Victor M. Bright, George M. Whitesides, “Surface Tension-Powered Self-Assembly of Microstructures – The State-of-the-Art”, *Journal of Microelectromechanical Systems*, Vol. 12, August 2003
- [5] P. W. Green, R. R. A. Syms, E. M. Yeatman, “Demonstration of Three-Dimensional Microstructure Self-Assembly”, *Journal of Microelectromechanical Systems*, Vol. 4, December 1995
- [6] His-Jen, J. Yeh, John S. Smith, “Fluidic Self-Assembly for the Integration of GaAs Light-Emitting Diodes on Si Substrates”, *IEEE Photonics technology letters*, Vol. 6, June 1994
- [7] Francis J. Hale, “Introduction to Control System Analysis and Design”, Prentice-Hall, Inc., Englewood Cliffs, New Jersey, 1973
- [8] Nils Napp, “Kinematic Parameter Estimation of Self-Assembling Systems via Photometric Stereo”, project work: EE 596 Advanced Topics in Signal and Image Processing, 2004

Websites:

- [9] <http://www.animalgenome.org/>, February 2006
- [10] <http://www.analog.com/>, February 2006
- [11] <http://www.silicondesigns.com/>, February 2006
- [12] <http://www.baumerelectric.com/>, February 2006
- [13] NIDAQ PCI 6025E: http://www.ni.com/pdf/products/us/4daqsc202-204_ETC_212-213.pdf, February 2006

8. APPENDIX

Appendix I: Graphs

Appendix II: Time planning

Appendix III: Drawings

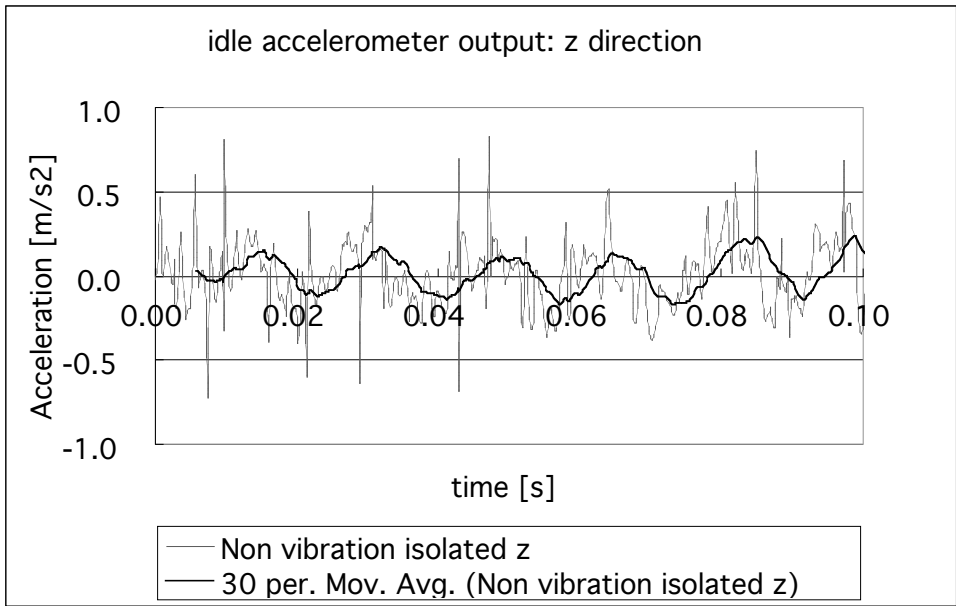
Appendix IV: Matlab simulation

Appendix V: Speaker specifications

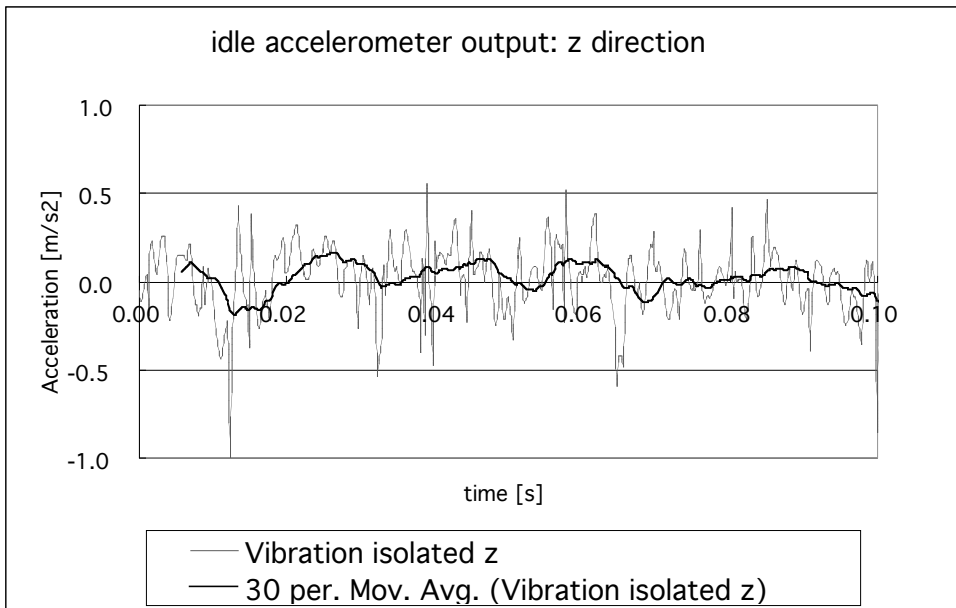
Appendix VI: Design of the cubes

Appendix VII: Accelerometer datasheet: ADXL321 / EBADXL321

Appendix I: Graphs



Plot 1: Accelerometer output on a non-vibration isolated table



Plot 2: Accelerometer output on a vibration isolated table

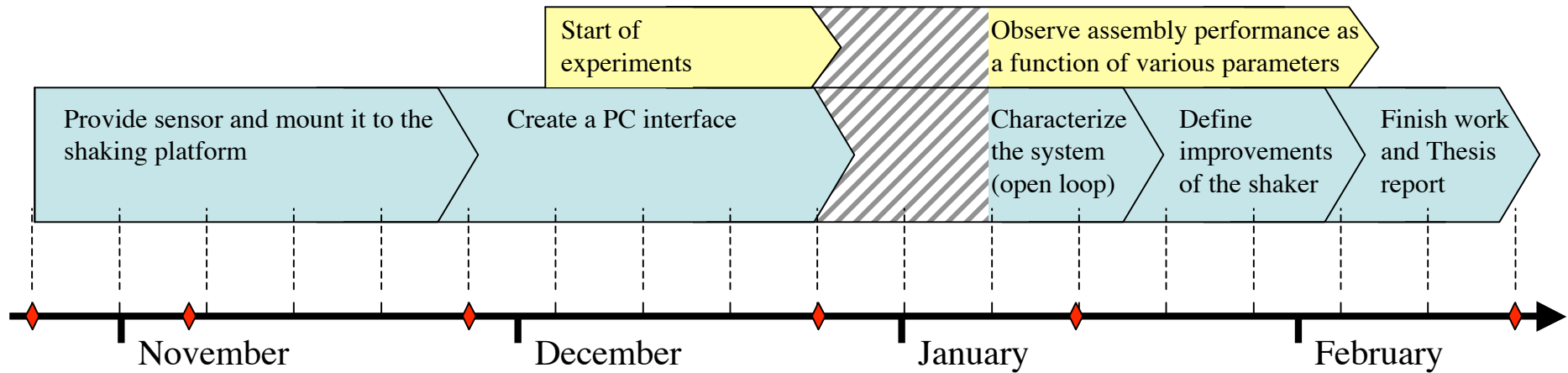
Plot 1 indicates that there is a noise signal:
 frequency ~ 50 Hz
 amplitude ~ 0.2 m/s²

The signal on the second plot has no regular pattern, but about the same amplitude.

Appendix II: Time planning

Time schedule

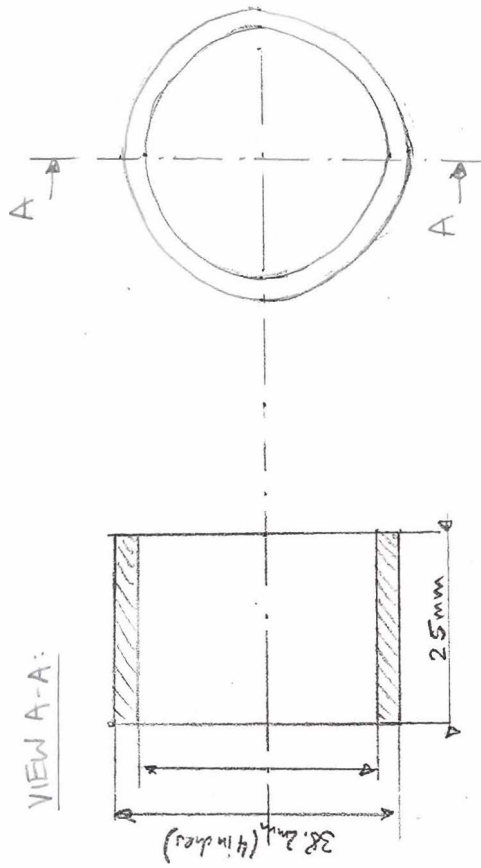
October 24th 2005- February 24th 2006



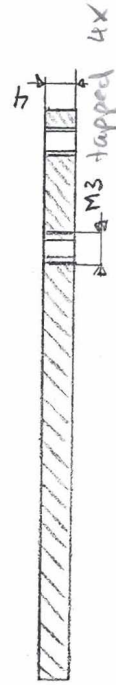
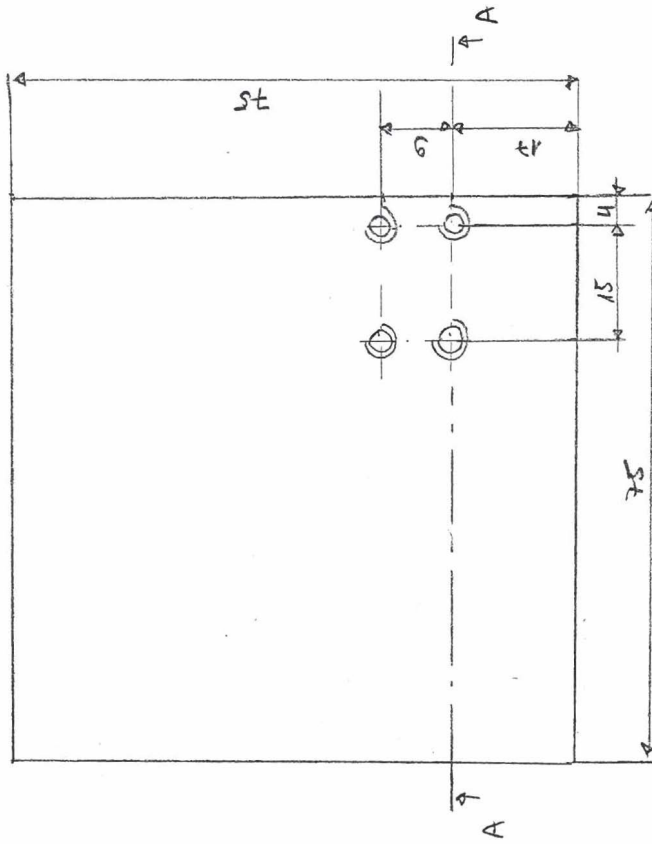
◆ Milestones:	
10-24-05	Project start
11-25-05	Sensor mounting, measurement of position
11-28-05	Start of experiments
12-23-05	Shaker interfced with the PC
01-12-06	Open loop characterization
02-23-06	Hand in report

- Experiments and modeling of self-assembly process
- Control of the shaker

Appendix III: Drawings

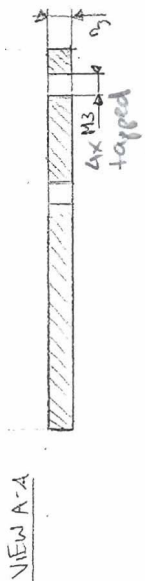
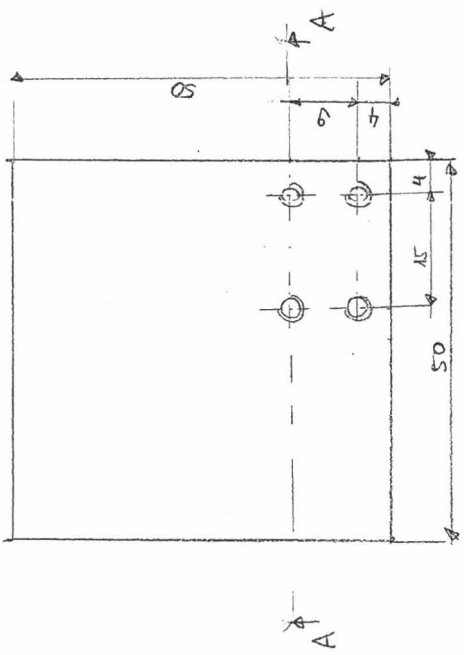


- ② 1 tube PLEXIGLAS
 MADELEINE KAGI
 kagi@ee.washington.edu
 SCALE 1:1
 mm



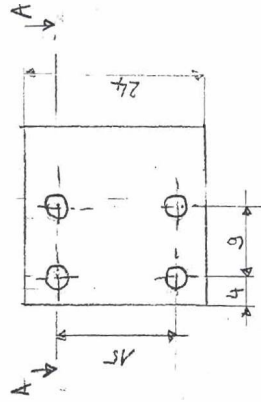
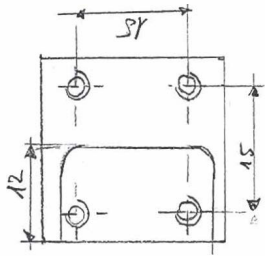
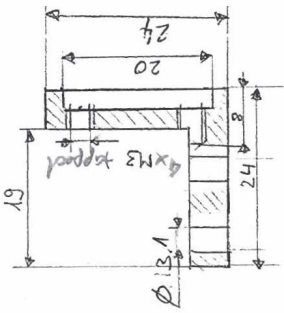
cut A-A:

- ③ 1 MAIN STAGE ALUMINUM
 MADELEINE KAGI
 kagi@ee.washington.edu
 (entity mm)
 scale 1:1

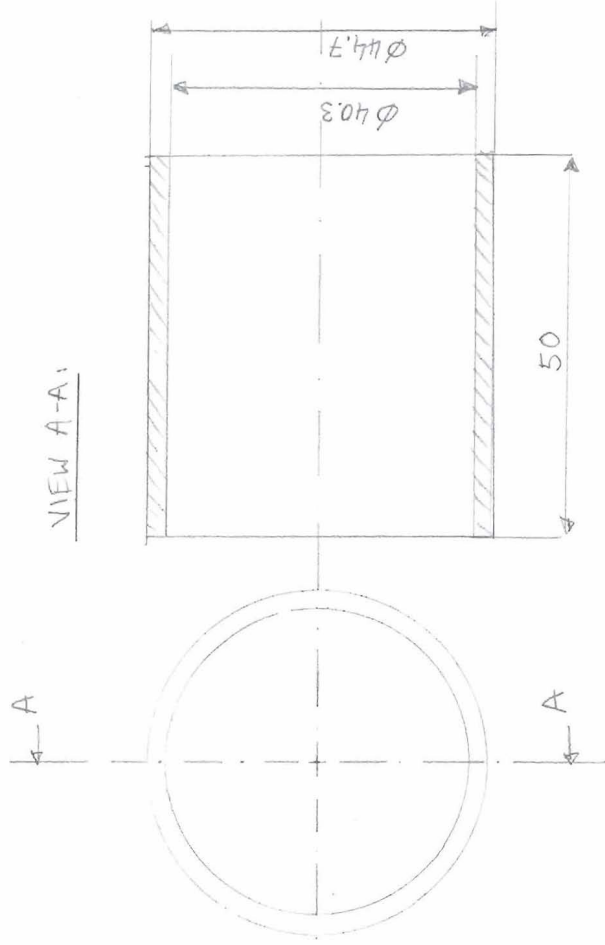


#3
 1 MAIN STAGE ALU MADELEINE
 MADELEINE KAGI
 kagi@ee.washington.edu
 SCALE 1:1
 mm

View A-A:



④ 1 ANGLE ALUMINIUM
MADELEINE KAGI
kagi@ee.washington.edu
SCALE 1:1
mm



- ⑦ 1 glass tube GLASS
 MADELEINE KAGI
 kagi@ee.washington.edu
 SCALE 1:1
 mm

Appendix IV: Matlab simulation

```

% KFB 3/3/04 adapted for 3D Self-Assembly: MK Jan/06
% simulate a point mass bouncing on a moving platform
% input: mass, initial position, initial velocity
%       coefficient of restitution alpha
% output: motion trace, energy of a point mass (kin. + pot.)
%%%%%%%%%%%%%%%%%%%%%%%%%%%%%%%%%%%%%%%%%%%%%%%%%%%%%%%%%%%%%%%%%%%%%%%%
% units and constants
g = 9.81;    % gravity

kg = 1;      % kilogram
gr = 1e-3;   % gram
mgr = 1e-6;  % milligram
ugr = 1e-9;  % microgram

m = 1;       % meter
mm = 1e-3;   % millimeter
um = 1e-6;   % micrometer

Hz = 1;      % hertz
kHz = 1e3;   % kilohertz

sec = 1;     % second
msec = 1e-3; % millisecond

%%%%%%%%%%%%%%%%%%%%%%%%%%%%%%%%%%%%%%%%%%%%%%%%%%%%%%%%%%%%%%%%%%%%%%%%
% system configuration
m1 = 0.597*ugr;
y1 = 100*um;
v1 = 0;

m2 = Inf;

A2 = 1.33*mm;    % amplitude of vibration
f = 19*Hz;       % frequency of vibration
omega = 2*pi*f;
v2_max = A2*omega; % maximum velocity
a2_max = A2*omega^2; % maximum acceleration

alpha = 0.36; % elasticity coefficient (1 - perfectly
elastic; 0 - perfectly plastic)
dt = 1*msec;
T = 0.5*sec;
Time = 0:dt:T;
%%%%%%%%%%%%%%%%%%%%%%%%%%%%%%%%%%%%%%%%%%%%%%%%%%%%%%%%%%%%%%%%%%%%%%%%
% simulation

n = size(Time,2); %returns the numbere of columns
Y1 = zeros(1,n); %posistion vectors
Y2 = zeros(1,n);
E = zeros(1,n);
Epot = zeros(1,n);

Y0 = []; V0 = [];

```

```

for i=1:n
    t = Time(i);
    y2 = A2*cos(omega*t);
    v2 = -A2*omega*sin(omega*t);
    if y1 < y2
        % m1 had impact with m2, need to compute new
        velocities
        if m2<Inf
            v1_new = (m1*v1 + m2*v2)/(m1+m2) +
alpha*m2/(m1+m2)*(v2-v1);
            %% v2_new = (m1*v1 + m2*v2)/(m1+m2) -
alpha*m1/(m1+m2)*(v2-v1); % here we assume v2 is given
        else
            v1_new = v2 + alpha*(v2-v1);
            v2_new = v2;
        end
        v1 = v1_new;
        %% v2 = v2_new;
        y1=y2; % hack to avoid m1 getting stuck under m2
        Y0 = [Y0 y1]; V0 = [V0 v1]; % keep track of initial
        position and velocity
    end
    % m1 in free flight
    y1_new = y1 + v1*dt - 1/2*g*dt*dt; % exact new position
    after dt
    v1_new = v1 - g*dt; % exact new velocity after dt
    Y1(i) = y1; Y2(i) = y2;
    y1 = y1_new; v1 = v1_new;
    E(i)=m1*(g*(y1)+0.5*(v1)*(v1));
end

figure(1);
if a2_max>g
    plot(Time,Y1,'.r',Time,Y2,'-');
else
    plot(Time,Y1,'.g',Time,Y2,'-');
end
xlabel('T [s]');
ylabel('y [m]');

Emax=max(E);
figure(2);
plot(Time,E,'r');
xlabel('T [s]');
ylabel('Energy [J]');
message = sprintf('max energy = %g J',Emax);
title(message);

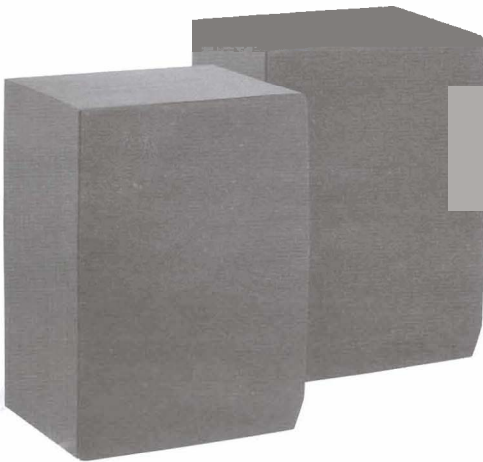
```

Appendix V: Speaker specifications

Presidian™

©2005, Innovation One Inc. All rights reserved. Innovation One and Presidian are trademarks used by Innovation One Inc.

Presidian 6.5" Bookshelf Speaker System PBS-5053

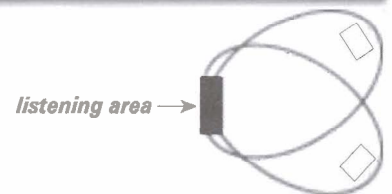


Thank you for purchasing the Presidian 6.5" inch Bookshelf Speaker System. Its space saving design lets you place your speakers on bookshelves or other small spaces. The 6.5-Inch High Compliance Woofer gives you excellent bass sound, while the 1/2-inch balanced Dome Tweeter gives you clear, clean and high-frequency sound.

1. Placing your speaker system

Listening area speaker placement

For the best stereo image, place a pair of speakers so the distance between them is about the same as the distance between the listening area and the point halfway between the speakers. If you must place the speakers farther apart, turn them slightly inward. If you must place them closer to each other, turn them slightly outward. Experiment with your speakers' placement to find the best location.

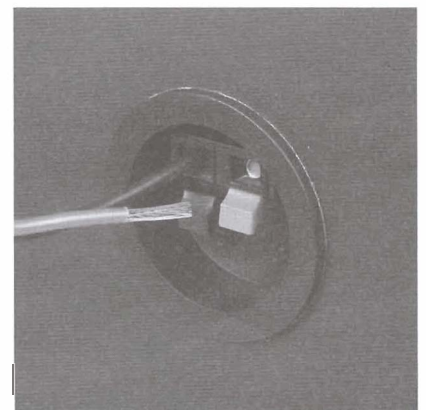


2. Connecting your speaker system

Connections

For the best performance, it is essential that you keep the speakers in the proper phase (connect + to + and - to -). We recommend using color-coded or marked wires to help you correctly connect the speakers to your sound system. Color-coded wires have stripes running down one side of the conductor's insulation; marked wires have ridges running along one side of the conductor's insulation.

1. Select a mounting location for the speakers that can withstand the speaker's weight and vibration.
2. Run speaker wire from the speakers to the receiver/amplifier.
3. Separate the wires about 4 inches at both ends. Strip 1/2-inch of insulation from the end of each conductor and twist.
4. Press the black (-) and red (+) terminal caps on the speakers to expose the holes in the terminals.
5. Insert the stripped wire ends into the holes in the terminals and release the terminals to secure the wires in place.
6. Connect the other ends of the wires to the matching terminals (- and +) on the receiver/amplifier.
7. Repeat steps 3-6 to connect your other speaker.



Cautions:

- Do not exceed the speakers' maximum power rating of 120 watts.
- To avoid damage to the speaker or amplifier/receiver, turn off the amplifier/receiver before making the connections.
- Use 18-gauge speaker wire (not supplied) for distances up to 50 feet. For greater distances, use 16-gauge wire (not supplied).

Caring for your speaker system

Keep the speakers dry. If your speakers get wet, wipe them dry immediately. Handle the speakers carefully. Do not drop them. Keep your speakers away from dust and dirt, and wipe them with a damp cloth occasionally to keep them looking new.

Cautions:

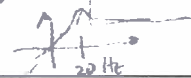
- You might permanently damage your speakers by cleaning them with a vacuum cleaner. Use a feather duster or a soft loose cloth instead.
- The warranty on these speakers is void if the voice coils are burned or damaged as a result of overpowering or clipping.

Specifications

Ø16.5cm

Speaker Compartment	6.5-Inch High Compliance Wool 1/2" Balanced Dome Tweeter
Frequency Response	65-20,000 Hz
Power Handling	50 Watts RMS
Maximum Power	100 Watts
.....	8 Ohms (Nominal)
Dimensions (HWD)	10.5 x 7.4 x 6.6 Inches (266 x 186 x 168 mm)
Weight.....	5.25 lb (2.4 kg)

Specifications are typical; individual units might vary. Specifications are subject to change and improvement without notice.



Service and repair

If your speakers are not performing as they should, take them to your local Innovation One dealer for assistance. To locate your nearest Innovation One dealer, call 1-866-249-4042. Modifying or tampering with the speakers internal components can cause a malfunction and might invalidate its warranty and void your FCC authorization to operate them.

Limited 90-day warranty

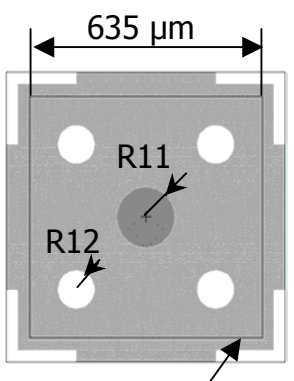
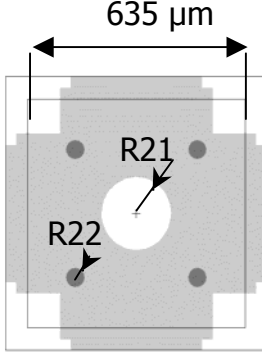
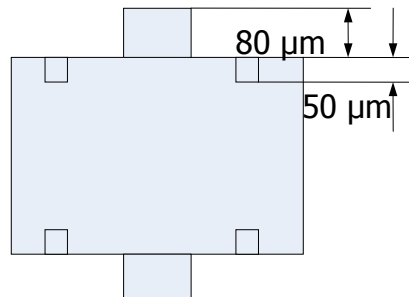
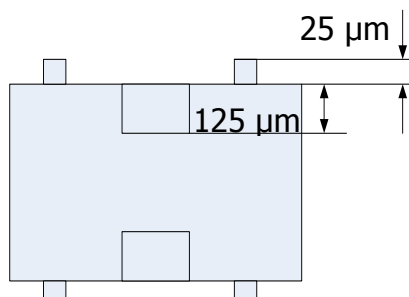
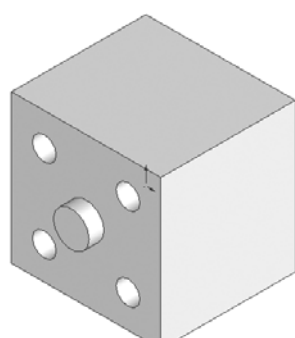
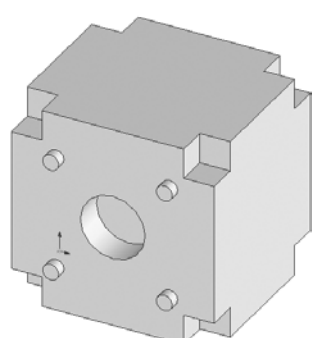
This product is warranted by Innovation One against manufacturing defects in material and workmanship under normal use for ninety (90) days from the date of purchase from authorized Innovation One dealers. EXCEPT AS PROVIDED HEREIN, Innovation One MAKES NO EXPRESS WARRANTIES AND ANY IMPLIED WARRANTIES, INCLUDING THOSE OF MERCHANTABILITY AND FITNESS FOR A PARTICULAR PURPOSE, ARE LIMITED IN DURATION TO THE DURATION OF THE WRITTEN LIMITED WARRANTIES CONTAINED HEREIN. EXCEPT AS PROVIDED HEREIN, Innovation One SHALL HAVE NO LIABILITY OR RESPONSIBILITY TO CUSTOMER OR ANY OTHER PERSON OR ENTITY WITH RESPECT TO ANY LIABILITY, LOSS OR DAMAGE CAUSED DIRECTLY OR INDIRECTLY BY USE OR PERFORMANCE OF THE PRODUCT OR ARISING OUT OF ANY BREACH OF THIS WARRANTY, INCLUDING; BUT NOT LIMITED TO, ANY DAMAGES RESULTING FROM INCONVENIENCE, LOSS OF TIME, DATA, PROPERTY, REVENUE, OR PROFIT OR ANY INDIRECT, SPECIAL, INCIDENTAL, OR CONSEQUENTIAL DAMAGES, EVEN IF Innovation One HAS BEEN ADVISED OF THE POSSIBILITY OF SUCH DAMAGES.

Some states do not allow limitations on how long an implied warranty lasts or the exclusion or limitation of incidental or consequential damages, so the above limitations or exclusions may not apply to you. In the event of a product defect during the warranty period, take the product and sales receipt as proof of purchase date to any Innovation One dealer. Innovation One will, at its option, unless otherwise provided by law: (a) correct the defect by product repair without charge for parts and labor; (b) replace the product with one of the same or similar design; or (c) refund the purchase price. All replaced parts and products, and products on which a refund is made, become the property of Innovation One. New or reconditioned parts and products may be used in the performance of warranty service. Repaired or replaced parts and products are warranted for the remainder of the original warranty period. You will be charged for repair or replacement of the product made after the expiration of the warranty period.

This warranty does not cover: (a) damage or failure caused by or attributable to acts of God, abuse, accident, misuse, improper or abnormal usage, failure to follow instructions, improper installation or maintenance, alteration, lightning or other incidence of excess voltage or current; (b) any repairs other than those provided by a Innovation One Authorized Service Facility; (c) consumables such as fuses or batteries; (d) cosmetic damage; (e) transportation, shipping or insurance costs; or (f) costs of product removal, installation, set-up service adjustment or reinstallation.

This warranty gives you specific legal rights, and you may also have other rights which vary from state to state.

Appendix VI: Design of the cubes

Type_1	Type_2
 <p>635 μm</p> <p>R11</p> <p>R12</p> <p>Effective area after dicing</p>	 <p>635 μm</p> <p>R21</p> <p>R22</p>
<p>R11 = 60 μm R12 = 40 μm</p>	<p>R21 = 80 μm R22 = 20 μm</p>
 <p>80 μm</p> <p>50 μm</p>	 <p>25 μm</p> <p>125 μm</p>
	

Appendix VII: Accelerometer datasheet:
ADXL321 / EBADXL321

FEATURES

Small and thin

- 4 mm \times 4 mm \times 1.45 mm LFCSP package
- 3 mg resolution at 50 Hz
- Wide supply voltage range: 2.4 V to 6 V
- Low power: 350 μA at $V_S = 2.4\text{ V}$ (typ)
- Good zero g bias stability
- Good sensitivity accuracy
- X-axis and Y-axis aligned to within 0.1° (typ)
- BW adjustment with a single capacitor
- Single-supply operation
- 10,000 g shock survival
- Compatible with Sn/Pb and Pb-free solder processes

APPLICATIONS

- Vibration monitoring and compensation
- Abuse event detection
- Sports equipment

GENERAL DESCRIPTION

The ADXL321 is a small and thin, low power, complete dual-axis accelerometer with signal conditioned voltage outputs, which is all on a single monolithic IC. The product measures acceleration with a full-scale range of $\pm 18\text{ g}$ (typical). It can also measure both dynamic acceleration (vibration) and static acceleration (gravity).

The ADXL321's typical noise floor is $320\ \mu\text{g}/\sqrt{\text{Hz}}$, allowing signals below 3 mg to be resolved in tilt-sensing applications using narrow bandwidths ($< 50\text{ Hz}$).

The user selects the bandwidth of the accelerometer using capacitors C_X and C_Y at the X_{OUT} and Y_{OUT} pins. Bandwidths of 0.5 Hz to 2.5 kHz may be selected to suit the application.

The ADXL321 is available in a very thin 4 mm \times 4 mm \times 1.45 mm, 16-lead, plastic LFCSP.

FUNCTIONAL BLOCK DIAGRAM

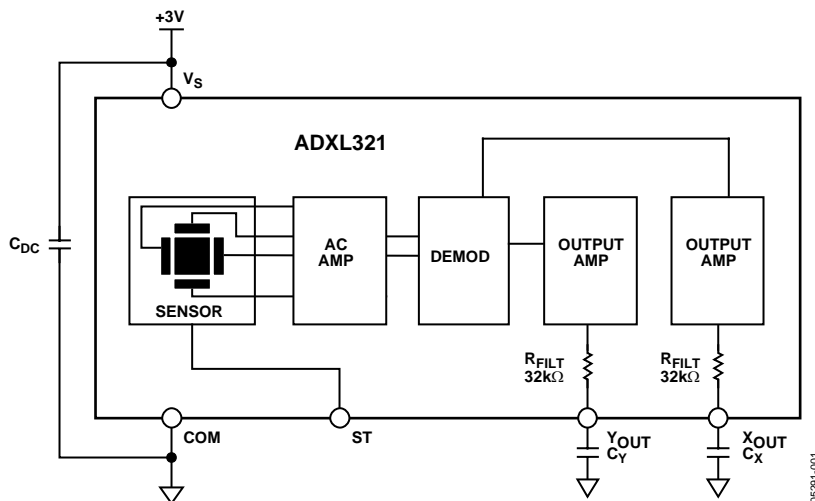


Figure 1.

Rev. 0

Information furnished by Analog Devices is believed to be accurate and reliable. However, no responsibility is assumed by Analog Devices for its use, nor for any infringements of patents or other rights of third parties that may result from its use. Specifications subject to change without notice. No license is granted by implication or otherwise under any patent or patent rights of Analog Devices. Trademarks and registered trademarks are the property of their respective owners.

TABLE OF CONTENTS

Specifications.....	3	Setting the Bandwidth Using C_X and C_Y	12
Absolute Maximum Ratings.....	4	Self-Test	12
ESD Caution.....	4	Design Trade-Offs for Selecting Filter Characteristics: The Noise/BW Trade-Off.....	12
Pin Configuration and Function Descriptions.....	5	Use with Operating Voltages Other than 3 V	13
Typical Performance Characteristics ($V_S = 3.0\text{ V}$)	7	Use as a Dual-Axis Tilt Sensor	13
Theory of Operation	11	Outline Dimensions	14
Performance	11	Ordering Guide	14
Applications.....	12		
Power Supply Decoupling	12		

REVISION HISTORY

12/04—Revision 0: Initial Version

SPECIFICATIONS¹

$T_A = 25^\circ\text{C}$, $V_S = 3\text{ V}$, $C_X = C_Y = 0.1\ \mu\text{F}$, Acceleration = 0 g, unless otherwise noted.

Table 1.

Parameter	Conditions	Min	Typ	Max	Unit
SENSOR INPUT					
Measurement Range	Each axis		± 18		g
Nonlinearity	% of full scale		± 0.2		%
Package Alignment Error			± 1		Degrees
Alignment Error	X sensor to Y sensor		± 0.1		Degrees
Cross Axis Sensitivity			± 2		%
SENSITIVITY (RATIOMETRIC)²					
Sensitivity at X_{OUT} , Y_{OUT}	$V_S = 3\text{ V}$	51	57	63	mV/g
Sensitivity Change due to Temperature ³	$V_S = 3\text{ V}$		0.01		%/ $^\circ\text{C}$
ZERO g BIAS LEVEL (RATIOMETRIC)					
0 g Voltage at X_{OUT} , Y_{OUT}	$V_S = 3\text{ V}$	1.4	1.5	1.6	V
0 g Offset vs. Temperature			± 2		mg/ $^\circ\text{C}$
NOISE PERFORMANCE					
Noise Density	@ 25°C		320		$\mu\text{g}/\sqrt{\text{Hz}}$ rms
FREQUENCY RESPONSE⁴					
C_X , C_Y Range ⁵		0.002		10	μF
R_{FILT} Tolerance			$32 \pm 15\%$		k Ω
Sensor Resonant Frequency			5.5		kHz
SELF-TEST⁶					
Logic Input Low			0.6		V
Logic Input High			2.4		V
ST Input Resistance to Ground			50		k Ω
Output Change at X_{OUT} , Y_{OUT}	Self-test 0 to 1		18		mV
OUTPUT AMPLIFIER					
Output Swing Low	No load		0.3		V
Output Swing High	No load		2.6		V
POWER SUPPLY					
Operating Voltage Range		2.4		6	V
Quiescent Supply Current			0.49		mA
Turn-On Time ⁷			20		ms
TEMPERATURE					
Operating Temperature Range		-20		+70	$^\circ\text{C}$

¹ All minimum and maximum specifications are guaranteed. Typical specifications are not guaranteed.

² Sensitivity is essentially ratiometric to V_S .

³ Defined as the change from ambient-to-maximum temperature or ambient-to-minimum temperature.

⁴ Actual frequency response controlled by user-supplied external capacitor (C_X , C_Y).

⁵ Bandwidth = $1/(2 \times \pi \times 32\text{ k}\Omega \times C)$. For C_X , $C_Y = 0.002\ \mu\text{F}$, bandwidth = 2500 Hz. For C_X , $C_Y = 10\ \mu\text{F}$, bandwidth = 0.5 Hz. Minimum/maximum values are not tested.

⁶ Self-test response changes cubically with V_S .

⁷ Larger values of C_X , C_Y increase turn-on time. Turn-on time is approximately $160 \times C_X$ or $C_Y + 4\text{ ms}$, where C_X , C_Y are in μF .

ABSOLUTE MAXIMUM RATINGS

Table 2.

Parameter	Rating
Acceleration (Any Axis, Unpowered)	10,000 <i>g</i>
Acceleration (Any Axis, Powered)	10,000 <i>g</i>
V _s	−0.3 V to +7.0 V
All Other Pins	(COM − 0.3 V) to (V _s + 0.3 V)
Output Short-Circuit Duration (Any Pin to Common)	Indefinite
Operating Temperature Range	−55°C to +125°C
Storage Temperature	−65°C to +150°C

Stresses above those listed under Absolute Maximum Ratings may cause permanent damage to the device. This is a stress rating only; functional operation of the device at these or any other conditions above those indicated in the operational section of this specification is not implied. Exposure to absolute maximum rating conditions for extended periods may affect device reliability.

ESD CAUTION

ESD (electrostatic discharge) sensitive device. Electrostatic charges as high as 4000 V readily accumulate on the human body and test equipment and can discharge without detection. Although this product features proprietary ESD protection circuitry, permanent damage may occur on devices subjected to high energy electrostatic discharges. Therefore, proper ESD precautions are recommended to avoid performance degradation or loss of functionality.



PIN CONFIGURATION AND FUNCTION DESCRIPTIONS

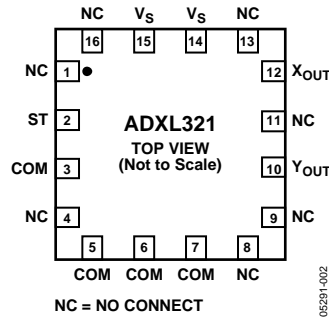


Figure 2. Pin Configuration

Table 3. Pin Function Descriptions

Pin No.	Mnemonic	Description
1, 4, 8, 9, 11, 13, 16	NC	Do Not Connect
2	ST	Self-Test
3, 5 to 7	COM	Common
10	Y _{OUT}	Y Channel Output
12	X _{OUT}	X Channel Output
14, 15	V _S	2.4 V to 6 V

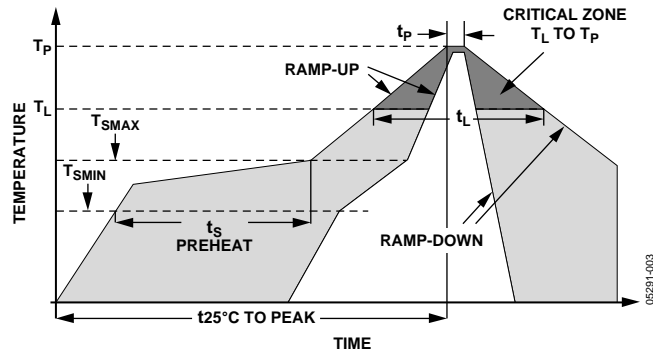


Figure 3. Recommended Soldering Profile

Table 4. Recommended Soldering Profile

Profile Feature	Sn63/Pb37	Pb-Free
Average Ramp Rate (T_L to T_P)	3°C/s max	3°C/s max
Preheat		
Minimum Temperature (T_{SMIN})	100°C	150°C
Minimum Temperature (T_{SMAX})	150°C	200°C
Time (T_{SMIN} to T_{SMAX}), t_s	60 s – 120 s	60 s – 150 s
T_{SMAX} to T_L		
Ramp-Up Rate	3°C/s	3°C/s
Time Maintained Above Liquidous (T_L)		
Liquidous Temperature (T_L)	183°C	217°C
Time (t_L)	60 s – 150 s	60 s – 150 s
Peak Temperature (T_P)	240°C + 0°C/-5°C	260°C + 0°C/-5°C
Time within 5°C of Actual Peak Temperature (t_p)	10 s – 30 s	20 s – 40 s
Ramp-Down Rate	6°C/s max	6°C/s max
Time 25°C to Peak Temperature	6 min max	8 min max

TYPICAL PERFORMANCE CHARACTERISTICS ($V_S = 3.0\text{ V}$)

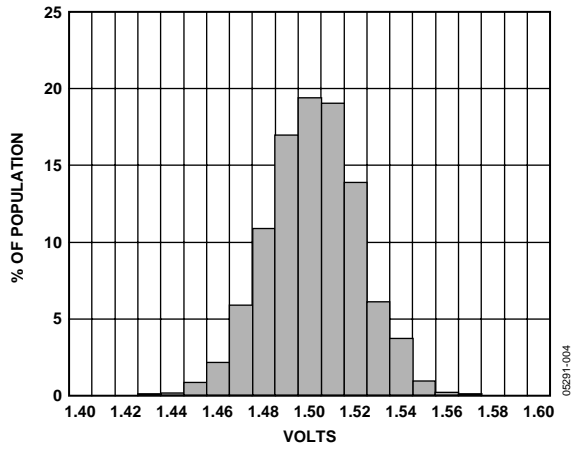


Figure 4. X-Axis Zero g Bias at 25°C

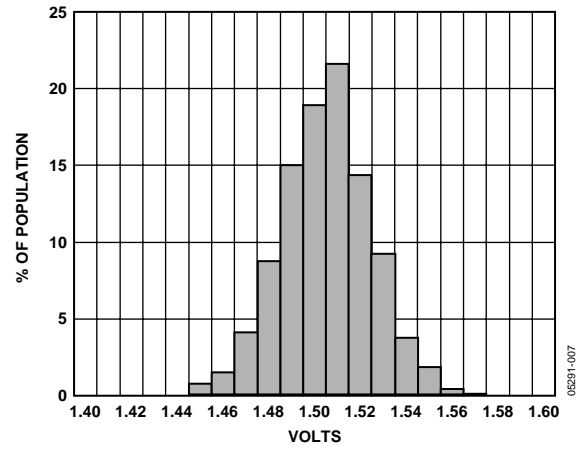


Figure 7. Y-Axis Zero g Bias at 25°C

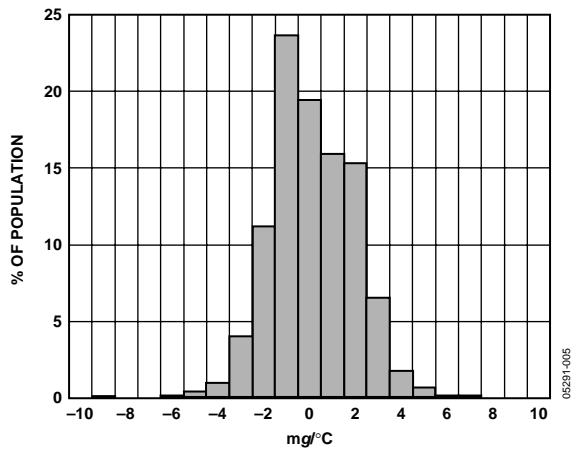


Figure 5. X-Axis Zero g Bias Temperature Coefficient

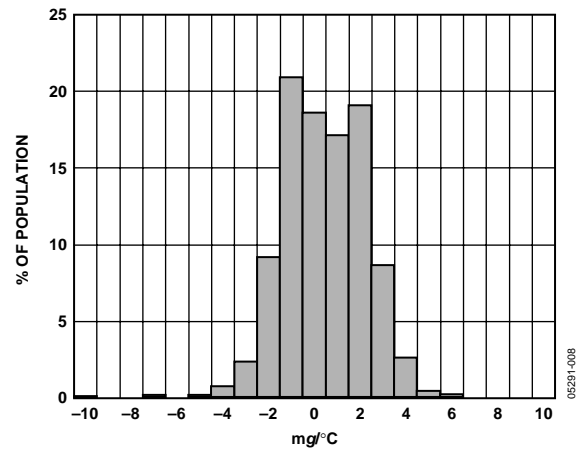


Figure 8. Y-Axis Zero g Bias Temperature Coefficient

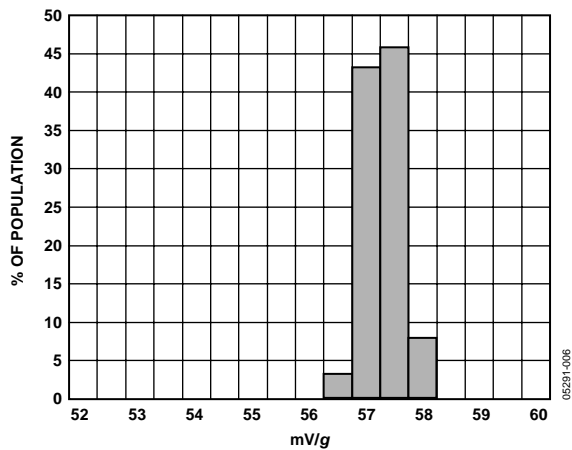


Figure 6. X-Axis Sensitivity at 25°C

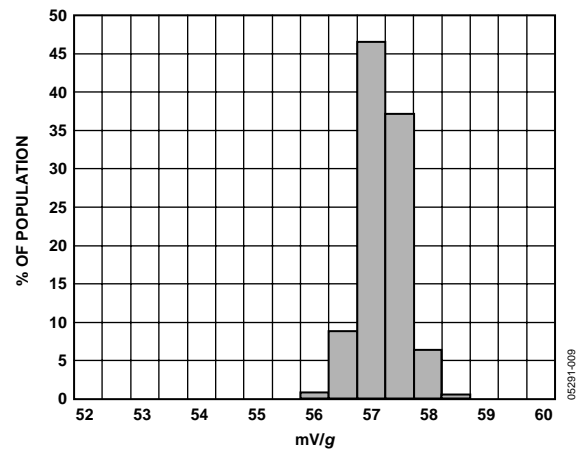


Figure 9. Y-Axis Sensitivity at 25°C

ADXL321

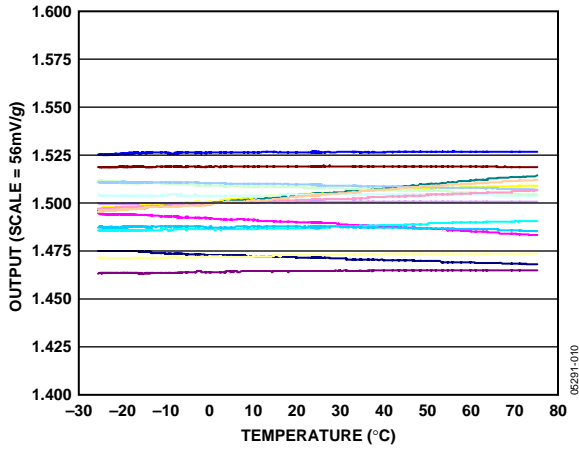


Figure 10. Zero g Bias vs. Temperature—Parts Soldered to PCB

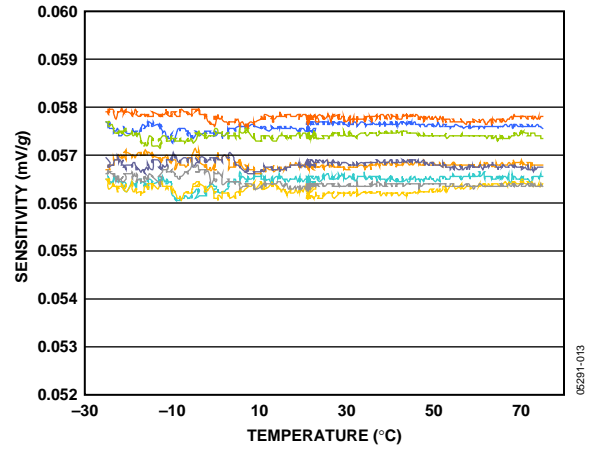


Figure 13. Sensitivity vs. Temperature—Parts Soldered to PCB

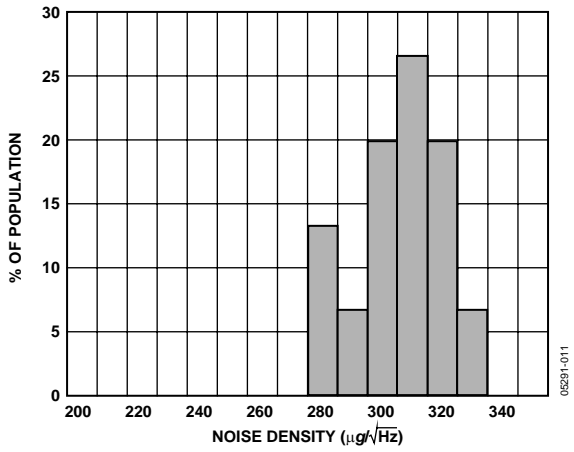


Figure 11. X-Axis Noise Density at 25°C

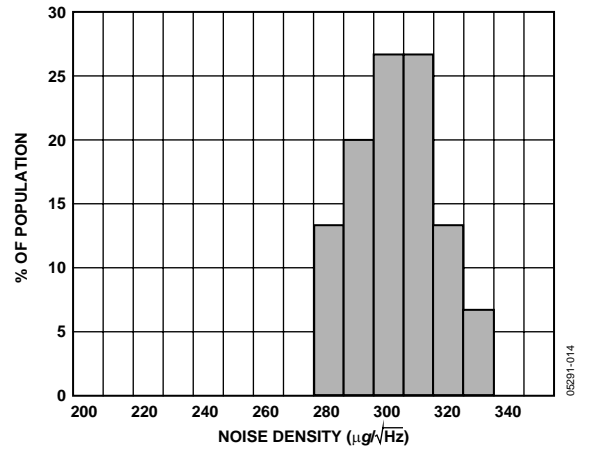


Figure 14. Y-Axis Noise Density at 25°C

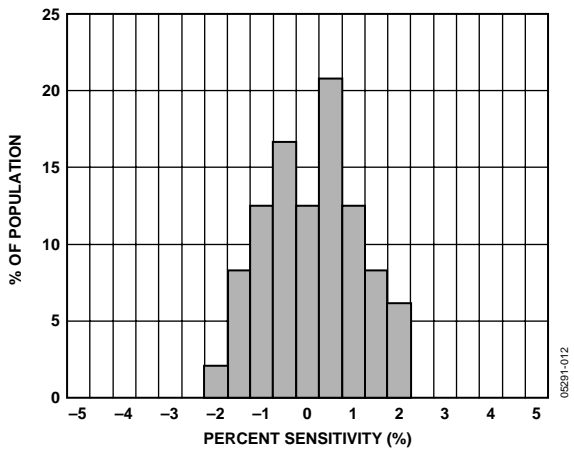


Figure 12. Z vs. X Cross-Axis Sensitivity

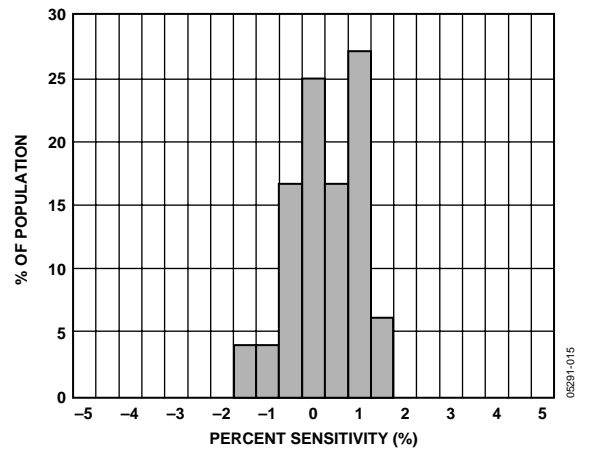


Figure 15. Z vs. Y Cross-Axis Sensitivity

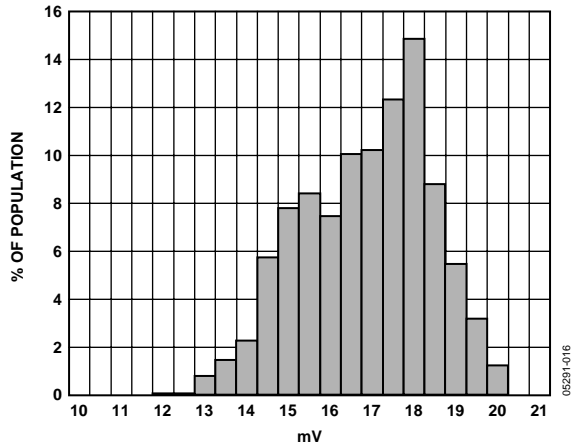


Figure 16. X-Axis Self-Test Response at 25°C

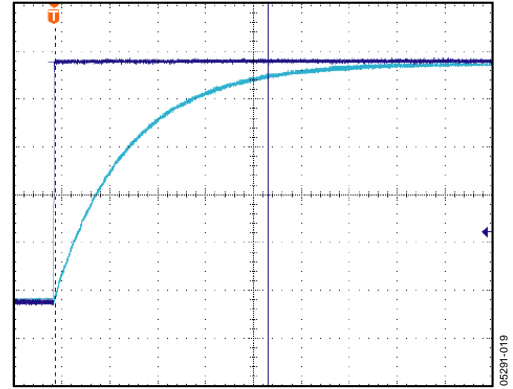


Figure 19. Turn-On Time— $C_x, C_y = 0.1 \mu F$, Time Scale = 2 ms/DIV

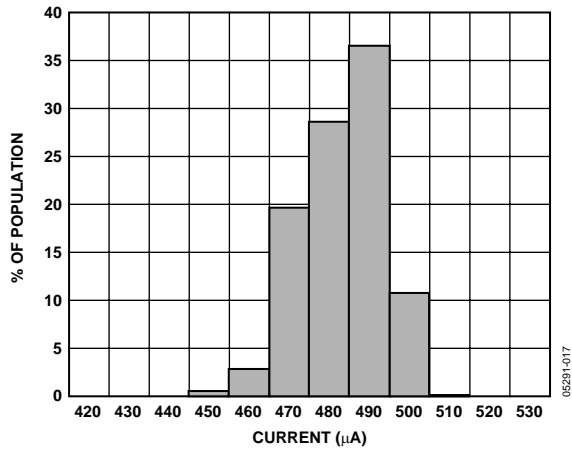


Figure 17. Supply Current at 25°C

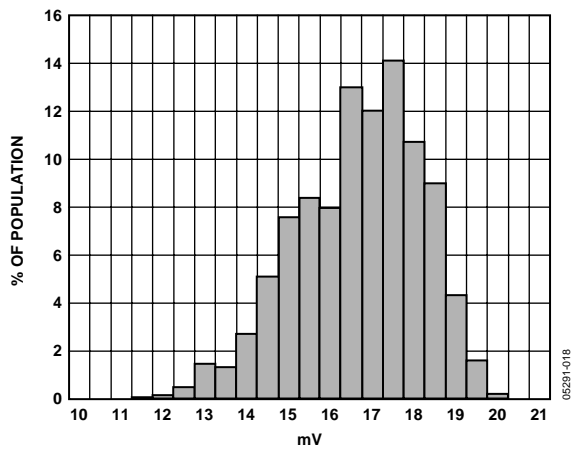


Figure 18. Y-Axis Self-Test Response at 25°C

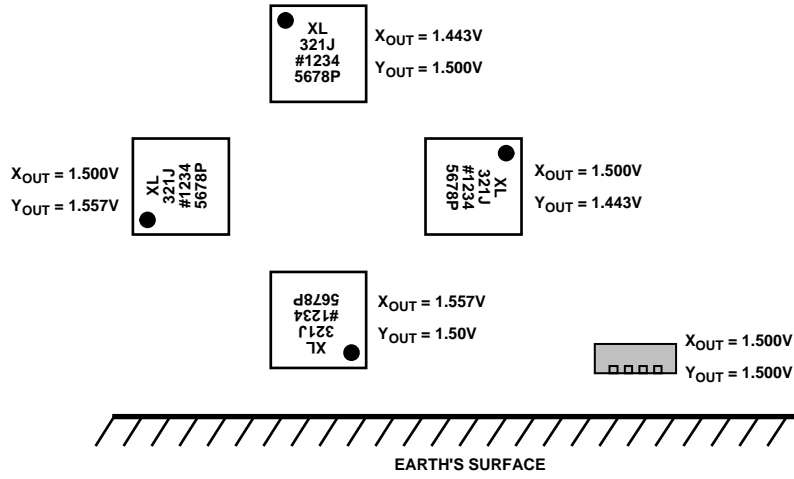


Figure 20. Output Response vs. Orientation (Top View)

THEORY OF OPERATION

The ADXL321 is a complete acceleration measurement system on a single monolithic IC. The ADXL321 has a measurement range of $\pm 18 g$. It contains a polysilicon surface-micromachined sensor and signal conditioning circuitry to implement an open-loop acceleration measurement architecture. The output signals are analog voltages that are proportional to acceleration. The accelerometer measures static acceleration forces, such as gravity, which allows it to be used as a tilt sensor.

The sensor is a polysilicon surface-micromachined structure built on top of a silicon wafer. Polysilicon springs suspend the structure over the surface of the wafer and provide a resistance against acceleration forces. Deflection of the structure is measured using a differential capacitor that consists of independent fixed plates and plates attached to the moving mass. The fixed plates are driven by 180° out-of-phase square waves. Acceleration deflects the beam and unbalances the differential capacitor, resulting in an output square wave whose amplitude is proportional to acceleration. Phase-sensitive demodulation techniques are then used to rectify the signal and determine the direction of the acceleration.

The demodulator's output is amplified and brought off-chip through a $32 k\Omega$ resistor. The user then sets the signal bandwidth of the device by adding a capacitor. This filtering improves measurement resolution and helps prevent aliasing.

PERFORMANCE

Rather than using additional temperature compensation circuitry, innovative design techniques have been used to ensure high performance is built-in. As a result, there is neither quantization error nor nonmonotonic behavior, and temperature hysteresis is very low (typically less than $10 mg$ over the $-20^\circ C$ to $+70^\circ C$ temperature range).

Figure 10 shows the zero g output performance of eight parts (X- and Y-axis) over a $-20^\circ C$ to $+70^\circ C$ temperature range.

Figure 13 demonstrates the typical sensitivity shift over temperature for supply voltages of $3 V$. This is typically better than $\pm 1\%$ over the $-20^\circ C$ to $+70^\circ C$ temperature range.

APPLICATIONS

POWER SUPPLY DECOUPLING

For most applications, a single 0.1 μF capacitor, C_{DC} , adequately decouples the accelerometer from noise on the power supply. However, in some cases, particularly where noise is present at the 140 kHz internal clock frequency (or any harmonic thereof), noise on the supply may cause interference on the ADXL321 output. If additional decoupling is needed, a 100 Ω (or smaller) resistor or ferrite bead may be inserted in the supply line. Additionally, a larger bulk bypass capacitor (in the 1 μF to 4.7 μF range) may be added in parallel to C_{DC} .

SETTING THE BANDWIDTH USING C_X AND C_Y

The ADXL321 has provisions for band-limiting the X_{OUT} and Y_{OUT} pins. Capacitors must be added at these pins to implement low-pass filtering for antialiasing and noise reduction. The equation for the 3 dB bandwidth is

$$F_{-3\text{dB}} = 1/(2\pi(32\text{ k}\Omega) \times C_{(X,Y)})$$

or more simply,

$$F_{-3\text{dB}} = 5\ \mu\text{F}/C_{(X,Y)}$$

The tolerance of the internal resistor (R_{FILT}) typically varies as much as $\pm 15\%$ of its nominal value (32 k Ω), and the bandwidth varies accordingly. A minimum capacitance of 2000 pF for C_X and C_Y is required in all cases.

Table 5. Filter Capacitor Selection, C_X and C_Y

Bandwidth (Hz)	Capacitor (μF)
1	4.7
10	0.47
50	0.10
100	0.05
200	0.027
500	0.01

SELF-TEST

The ST pin controls the self-test feature. When this pin is set to V_S , an electrostatic force is exerted on the accelerometer beam. The resulting movement of the beam allows the user to test if the accelerometer is functional. The typical change in output is 315 mg (corresponding to 18 mV). This pin may be left open-circuit or connected to common (COM) in normal use.

The ST pin should never be exposed to voltages greater than $V_S + 0.3\text{ V}$. If this cannot be guaranteed due to the system design (for instance, if there are multiple supply voltages), then a low V_F clamping diode between ST and V_S is recommended.

DESIGN TRADE-OFFS FOR SELECTING FILTER CHARACTERISTICS: THE NOISE/BW TRADE-OFF

The accelerometer bandwidth selected ultimately determines the measurement resolution (smallest detectable acceleration). Filtering can be used to lower the noise floor, which improves the resolution of the accelerometer. Resolution is dependent on the analog filter bandwidth at X_{OUT} and Y_{OUT} .

The output of the ADXL321 has a typical bandwidth of 2.5 kHz. The user must filter the signal at this point to limit aliasing errors. The analog bandwidth must be no more than half the A/D sampling frequency to minimize aliasing. The analog bandwidth may be further decreased to reduce noise and improve resolution.

The ADXL321 noise has the characteristics of white Gaussian noise, which contributes equally at all frequencies and is described in terms of $\mu\text{g}/\sqrt{\text{Hz}}$ (the noise is proportional to the square root of the accelerometer's bandwidth). The user should limit bandwidth to the lowest frequency needed by the application in order to maximize the resolution and dynamic range of the accelerometer.

With the single-pole, roll-off characteristic, the typical noise of the ADXL321 is determined by

$$rmsNoise = (320\ \mu\text{g}/\sqrt{\text{Hz}}) \times (\sqrt{\text{BW} \times 1.6})$$

At 100 Hz bandwidth the noise will be

$$rmsNoise = (320\ \mu\text{g}/\sqrt{\text{Hz}}) \times (\sqrt{100 \times 1.6}) = 4\text{ mg}$$

Often, the peak value of the noise is desired. Peak-to-peak noise can only be estimated by statistical methods. A factor of 6 is generally used to convert rms to peak-to-peak. Table 6 is useful for estimating the probabilities of exceeding various peak values, given the rms value.

Table 6. Estimation of Peak-to-Peak Noise

Peak-to-Peak Value	% of Time That Noise Exceeds Nominal Peak-to-Peak Value
$2 \times rms$	32
$4 \times rms$	4.6
$6 \times rms$	0.27
$8 \times rms$	0.006

Peak-to-peak noise values give the best estimate of the uncertainty in a single measurement. Table 7 gives the typical noise output of the ADXL321 for various C_X and C_Y values.

Table 7. Filter Capacitor Selection (C_X , C_Y)

Bandwidth (Hz)	C_X , C_Y (μF)	RMS Noise (mg)	Peak-to-Peak Noise Estimate (mg)
10	0.47	1.3	7.8
50	0.1	2.9	17.4
100	0.047	4	24
500	0.01	9.1	54.6

USE WITH OPERATING VOLTAGES OTHER THAN 3 V

The ADXL321 is tested and specified at $V_S = 3\text{ V}$; however, it can be powered with V_S as low as 2.4 V or as high as 6 V. Note that some performance parameters change as the supply voltage is varied.

The ADXL321 output is ratiometric, so the sensitivity (or scale factor) varies proportionally to supply voltage. At $V_S = 5\text{ V}$, the sensitivity is typically 100 mV/g. At $V_S = 2.4\text{ V}$, the sensitivity is typically 45 mV/g.

The zero g bias output is also ratiometric, so the zero g output is nominally equal to $V_S/2$ at all supply voltages.

The output noise is not ratiometric but is absolute in volts; therefore, the noise density decreases as the supply voltage increases. This is because the scale factor (mV/g) increases while the noise voltage remains constant. At $V_S = 5\text{ V}$, the noise density is typically $190\ \mu\text{g}/\sqrt{\text{Hz}}$, while at $V_S = 2.4\text{ V}$, the noise density is typically $400\ \mu\text{g}/\sqrt{\text{Hz}}$.

Self-test response in g is roughly proportional to the square of the supply voltage. However, when ratiometricity of sensitivity is factored in with supply voltage, the self-test response in volts is roughly proportional to the cube of the supply voltage. For example, at $V_S = 5\text{ V}$, the self-test response for the ADXL321 is approximately 80 mV. At $V_S = 2.4\text{ V}$, the self-test response is approximately 8 mV.

The supply current decreases as the supply voltage decreases. Typical current consumption at $V_S = 5\text{ V}$ is 750 μA , and typical current consumption at $V_S = 2.4\text{ V}$ is 350 μA .

USE AS A DUAL-AXIS TILT SENSOR

An accelerometer is most sensitive to tilt when its sensitive axis is perpendicular to the force of gravity (that is, when it is parallel to the earth's surface). At this orientation, its sensitivity to changes in tilt is highest. When the accelerometer is oriented on axis to gravity (near its +1 g or -1 g reading), the change in output acceleration per degree of tilt is negligible. When the accelerometer is perpendicular to gravity, its output changes nearly 17.5 mg per degree of tilt. At 45°, its output changes at only 12.2 mg per degree of tilt, and resolution declines.

Converting Acceleration to Tilt

When the accelerometer is oriented so both its X-axis and Y-axis are parallel to the earth's surface, it can be used as a 2-axis tilt sensor with both a roll axis and pitch axis. Once the output signal from the accelerometer has been converted to an acceleration that varies between -1 g and +1 g, the output tilt in degrees is calculated as

$$PITCH = \arcsine(A_X/1\text{ g})$$

$$ROLL = \arcsine(A_Y/1\text{ g})$$

Be sure to account for overranges. It is possible for the accelerometers to output a signal greater than $\pm 1\text{ g}$ due to vibration, shock, or other accelerations.

ADXL321

OUTLINE DIMENSIONS

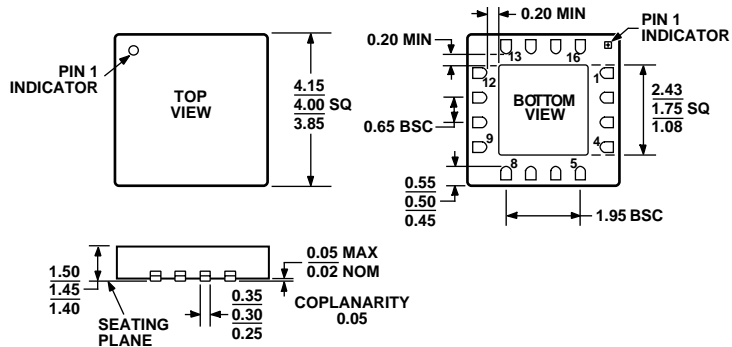


Figure 21. 16-Lead Lead Frame Chip Scale Package [MQ_LFCSP]
 4 mm × 4 mm Body, Thick Quad (CP-16-5)
 Dimensions shown in millimeters
 (Drawing Not to Scale)

ORDERING GUIDE

Model	Measurement Range	Specified Voltage (V)	Temperature Range	Package Description	Package Option
ADXL321JCP ¹	±18 g	3	−20°C to +70°C	16-Lead LFCSP	CP-16-5
ADXL321JCP-REEL ¹	±18 g	3	−20°C to +70°C	16-Lead LFCSP	CP-16-5
ADXL321EB				Evaluation Board	

¹ Lead finish—Matte tin.

NOTES

ADXL321

NOTES

GENERAL DESCRIPTION

The ADXL321EB is a simple evaluation board that allows quick evaluation of the performance of the ADXL321 dual-axis $\pm 18\text{ g}$ accelerometer. The ADXL321EB has a 5-pin, 0.1 inch spaced header for access to all power and signal lines which the user can attach to a prototyping board (breadboard) or wire using a standard plug. Four holes are provided for mechanical attachment of the ADXL321EB to the application.

The ADXL321EB is 20 mm \times 20 mm, with mounting holes set 15 mm \times 15 mm at the corners of the PCB.

CIRCUIT DESCRIPTION

The schematic of the ADXL321EB is shown in Figure 1. Analog bandwidth can be set by changing capacitors C2 and C3. See the ADXL321 data sheet for a complete description of the operation of the accelerometer.

The part layout of the ADXL321EB is shown in Figure 2. The ADXL321EB has two factory-installed 100 nF capacitors (C2 and C3) at X_{OUT} and Y_{OUT} to reduce the bandwidth to 50 Hz. Many applications require a different bandwidth, in which case the user can change C2 and C3, as appropriate.

SPECIAL NOTES ON HANDLING

The ADXL321EB is not reverse polarity protected. Reversing the +V supply and ground pins can cause damage to the ADXL321.

Dropping the ADXL321EB on a hard surface can generate several thousand g of acceleration and might exceed the data sheet absolute maximum limits. See the ADXL321 data sheet for more information.

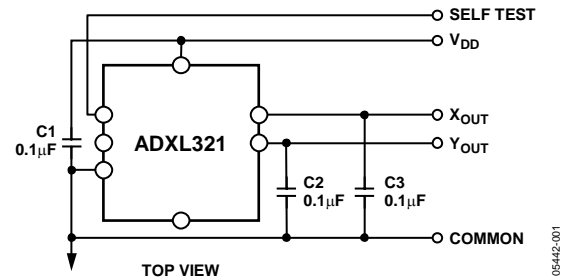


Figure 1. ADXL321EB Schematic

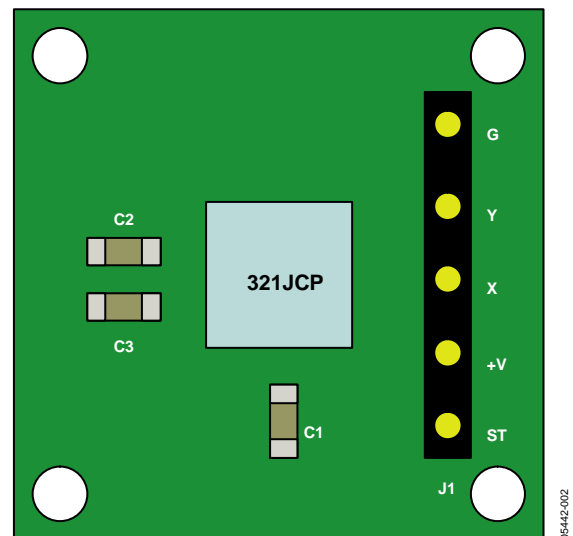


Figure 2. ADXL321EB Physical Layout

ORDERING GUIDE

Model	Package Description
ADXL321EB	Evaluation Board

Rev. 0

Information furnished by Analog Devices is believed to be accurate and reliable. However, no responsibility is assumed by Analog Devices for its use, nor for any infringements of patents or other rights of third parties that may result from its use. Specifications subject to change without notice. No license is granted by implication or otherwise under any patent or patent rights of Analog Devices. Trademarks and registered trademarks are the property of their respective owners.

ADXL321EB

NOTES